A linearized theory for rotational supercavitating flow

By ROBERT L. STREET

Department of Civil Engineering, Stanford University

(Received 18 January 1963)

In this paper methods are given for establishing qualitative and quantitative measures of the effects of rotation in supercavitating flows past slender bodies. A linearized theory is developed for steady, two-dimensional flow under the assumption that the flow has a constant rotation throughout. The stream function of the rotational flow satisfies Poisson's equation. By using a particular solution of this equation, the rotational problem is reduced to a problem involving Laplace's equation and harmonic perturbation velocities. The resulting boundary-value problem is solved by use of conformal mapping and singularities from thin-airfoil theory. The theory is then applied to asymmetric shear flow past wedges and hydrofoils and to symmetric shear flow past wedges. The presence of rotation is shown to create significant changes in the forces acting on the slender bodies and in the shape and size of the trailing cavities.

1. Introduction

Cavitation occurs in a fluid flow as a consequence of local pressure reduction, usually brought about by high local velocities. The development of high-speed submarines, underwater missiles, and other vehicles, together with the surface-piercing hydrofoil ship, has renewed interest in the large-scale effects of cavitation. The hydrofoil and wedge (or strut) are practical parts of the total hydrodynamic system of most of these vehicles. In many cases these parts are long and slender and, at sufficiently high speeds, produce long, trailing, steady-state cavities. The characteristics of these so-called supercavitating flows are of particular interest to the design engineer. When the cavity pressure does not differ greatly from the free-stream pressure, the velocities near the body and cavity are not greatly different from the free-stream speed. It is possible, then, to study the two-dimensional flows by means of a linearized theory based on the well-known theory of thin airfoils.

In linearized, two-dimensional theory the effects of viscosity are usually neglected. The flow is then assumed to be irrotational and the velocity to be uniform at points far from the slender body. However, since no fluid is completely inviscid, all real flows are rotational. Even when viscosity is neglected, the flow picture may sometimes be best represented by a rotational flow.

Many rotational flows have already been studied empirically and analytically. The rotational flows studied by Yih (1959) are of particular interest because his results show the importance of vorticity in reproducing physical effects. He considers the steady, rotational flow of an inviscid fluid in a two-dimensional

channel or in a circular tube toward a sink. His solutions show the unusual (for inviscid theory) features of separating streamlines and corner eddies similar to those found in the real viscous flows. Tsien (1943) recognized that in many applications of two-dimensional airfoil theory, irrotational flow conditions are not satisfied. He states in his paper on airfoils in shear flow that, for example, the large vertical velocity gradient near the ground can be approximated to the first order by a flow with a linear velocity distribution (a shear flow).

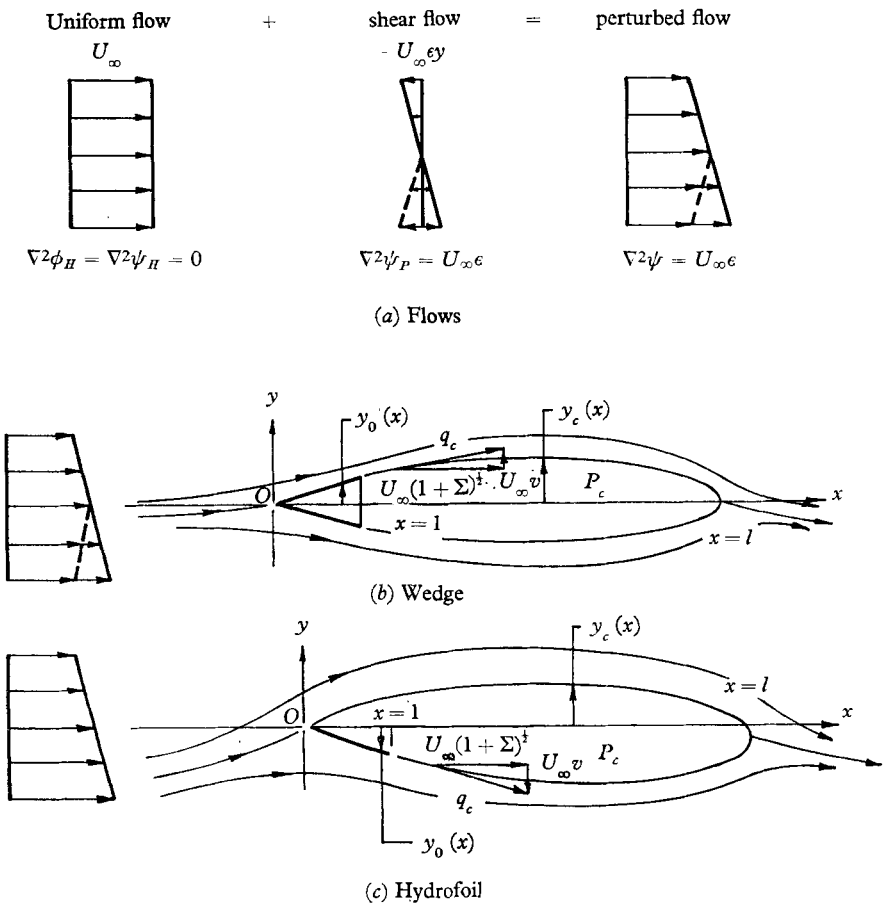

FIGURE 1. Velocity distributions and fully cavitated flows.

The present work may be regarded as an extension of both Tulin's linearized theory for supercavitating flow (1953) and Tsien's method for rotational, non-cavitating flow. The effects of gravity and surface tension are specifically neglected, while the effects of viscosity are modelled by the rotational flow. In the study a uniform, parallel, irrotational flow is perturbed by a uniform shear flow—a flow with constant vorticity. The vorticity is presumed to have come from some upstream disturbance, e.g. a boundary layer developing on the body of a vessel or on test-tunnel walls. Hydrofoils and struts that lie in the slip-stream or wake of other components would be in such a vortex field.

The perturbed flow and the physical problems to be studied are shown in figures 1 and 2. The perturbed flow is a uniform shear flow characterized by a linear velocity distribution. Both the rotational perturbed and the irrotational flows satisfy the equation of continuity; therefore, the stream function ψ exists in both. However, the velocity potential ϕ can, of course, exist only in the irrotational flow. Only steady, two-dimensional flows are studied; the fluid is of infinite extent and has a constant density ρ. The flow detaches at the leading and trailing edges of the hydrofoil and at both edges of the blunt base of the symmetric wedge. Finally, the cavity length, when measured from the leading edge of the body, is greater than that of the solid body, i.e. full cavitation occurs.

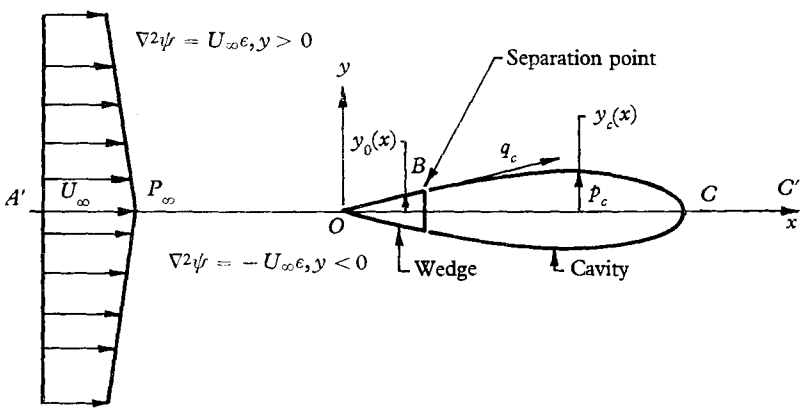

FIGURE 2. Symmetric shear flow past a wedge.

2. The linearized theory

The linearized theory is developed under the assumption that the supercavitating flows have a constant vorticity throughout. Because of its simplicity and convenience, Tulin's closed-cavity model is employed; however, other linearized models are available (see Geurst 1961 and Fabula 1962). Figure 1 shows typical flows. The unit-length body is used without loss of generality, since it is equivalent to normalizing the problem on the actual body length. Although it is certainly disturbed in the neighbourhood of the slender body, the basic flow is assumed to be undisturbed at infinity and is characterized there by a constant vorticity. The wedge is aligned in the flow with its longitudinal centreline parallel to the x-axis, while the hydrofoil is placed at an angle of attack α with respect to the x-axis.

The shear velocity profile at $x = -\infty$ is $U_\infty[1 - \epsilon y/\text{chord}]$, where U_∞ represents the velocity at $(-\infty, 0)$ and $(U_\infty\epsilon/\text{chord})$ is the vorticity at infinity. From these definitions it follows that the relative vorticity ϵ is non-dimensional; it remains so even though the unit chord of the solid body is not shown specifically in the following development. The pressure at infinity is the undisturbed static pressure p_∞. The flow velocities U and V are in the x- and y-directions, respectively, while the velocity at any point is q and the velocity on the cavity surfaces is q_c. The closed, trailing cavity is characterized by a length l greater than one, an

ordinate $y_c(x)$, and a constant pressure p_c. It is presumed that the cavity is filled with air or water vapour.

In a two-dimensional flow, the vorticity component is $\zeta = \partial V/\partial x - \partial U/\partial y$ and the rotation is $\omega = \frac{1}{2}\zeta$. Since the flow has a constant vorticity $\zeta = U_\infty \epsilon$ at infinity, it follows from the Helmholtz theorem on the permanence of rotation that the vorticity persists throughout the fluid; thus

$$\frac{\partial V}{\partial x} - \frac{\partial U}{\partial y} = U_\infty \epsilon. \tag{2.1}$$

Furthermore, the continuity equation

$$\frac{\partial U}{\partial x} + \frac{\partial V}{\partial y} = 0 \tag{2.2}$$

must be satisfied throughout the fluid. In this rotational flow a stream function $\psi(x, y)$, which satisfies equation (2.2) identically, exists and may be defined so that

$$U = -\frac{\partial \psi}{\partial y}, \quad V = \frac{\partial \psi}{\partial x}. \tag{2.3}$$

Poisson's equation

$$\nabla^2 \psi(x, y) = U_\infty \epsilon \tag{2.4}$$

is produced when ψ is introduced into equation (2.1). Finally, the Bernoulli equation for steady two-dimensional flow with constant vorticity (or rotation) is

$$p + \tfrac{1}{2}\rho q^2 - \rho U_\infty \epsilon \psi = \text{const.} \tag{2.5}$$

By the use of superposition, the solution to equation (2.4) can be written as $\psi = \psi_H + \psi_P$, with $\nabla^2 \psi_H = 0$ and $\nabla^2 \psi_P = U_\infty \epsilon$. The stream function ψ_H represents a new harmonic flow; ψ_P is a particular solution of equation (2.4). From equation (2.3), then

$$\left.\begin{aligned} U(x, y) &= U_H(x, y) + U_P(x, y), \\ V(x, y) &= V_H(x, y) + V_P(x, y). \end{aligned}\right\} \tag{2.6}$$

If one selects $\psi_P = \frac{1}{2} U_\infty \epsilon y^2$, then

$$U = U_H - U_\infty \epsilon y \quad \text{and} \quad V = V_H.$$

It is evident that any problem that requires a solution for U and V can be reduced to an equivalent problem for the harmonic velocities U_H and V_H.

The boundary conditions on the solid body and cavity walls and a compatible boundary-value problem are established in terms of a linearized theory. The flow pattern is a combination of a parallel, uniform, shear flow and, superposed on this, small velocity perturbations. The flow velocities are written in terms of the non-dimensional, harmonic perturbation velocities (u, v) in the x- and y-directions, respectively. From equation (2.6)

$$U = U_\infty(1 + u - \epsilon y) \quad \text{and} \quad V = U_\infty v \tag{2.6a}$$

in the linearized flow. In a linearized theory it is assumed that the perturbation velocities (u, v), the attack (or wedge semi) angle α, the body shape (or camber) $y_0(x)$, and the cavity ordinate $y_c(x)$ are small. First-order terms in these quantities

are retained, but second- and higher-order terms are neglected. In the present rotational development, terms of the form ϵy_c arise in the boundary conditions for the perturbation velocities; in order to preserve the first-order smallness of these velocities, it is necessary to restrict the relative vorticity ϵ to a size of the order of one. In this case, then, the flow reversal, which occurs in a uniform shear flow at $y \approx 1/\epsilon$, does not occur near the body-cavity combination, whose ordinates are usually very small compared to one. Finally, from the Cauchy–Riemann equations as applied to the harmonic perturbation velocities, it is seen that these velocities change very slowly in space when the streamline slopes and curvatures are small (Tulin 1953). For this reason the linearized boundary conditions are applied on the x-axis rather than on the surfaces of the slender body-cavity combination.

Recalling that $\psi = \psi_H + (\frac{1}{2}\epsilon U_\infty y^2)$, one has, from equation (2.5),

$$\frac{p_\infty - p_c}{\frac{1}{2}\rho U_\infty^2} + \frac{2\epsilon \tilde{\psi}_H}{U_\infty} + \epsilon^2 y_\infty^2 = \frac{q_c^2}{U_\infty^2} - 1 = \text{const.}$$

The stream function $\tilde{\psi}_H$ represents the difference between the harmonic stream-function value on the x-axis and its value on the upstream extension of the cavity streamline. Thus, $\tilde{\psi}_H = -U_\infty y_\infty$, where y_∞ is the ordinate of the stagnation streamline at $x = -\infty$ and its value is not known *a priori*. In these rotational flows the cavitation number σ, defined in the usual sense as

$$\sigma = \frac{p_\infty - p_c}{\frac{1}{2}\rho U_\infty^2}, \tag{2.7}$$

cannot be used directly since

$$\sigma = \frac{q_c^2}{U_\infty^2} - 1 + 2\epsilon y_\infty - \epsilon^2 y_\infty^2,$$

where y_∞ is unknown. Therefore, it is convenient to define a rotational cavitation number

$$\Sigma = q_c^2/U_\infty^2 - 1. \tag{2.7a}$$

When either $\epsilon \to 0$ or the flow is symmetric, then $\Sigma = \sigma$; otherwise,

$$\sigma = \Sigma + \epsilon y_\infty (2 - \epsilon y_\infty).$$

This relationship provides a means for relating the pressure differences and flow velocities in experimental programmes.

On the cavity walls the velocity q_c is constant for a given ϵ. Writing q_c in terms of the perturbation velocities and introducing the result into equation (2.7a) yields, after linearization, the cavity boundary condition

$$u(x, 0) = \tfrac{1}{2}\Sigma + \epsilon y_c(x) \quad (a \leqslant x \leqslant l). \tag{2.8}$$

When equation (2.8) is applied to the upper cavity surface in a flow past a hydrofoil, $a = 0$; otherwise, $a = 1$ for flows past wedges and hydrofoils. Furthermore, if one lets $U_c = U_\infty(1 + u - \epsilon y_c)$ on the cavity, then $q_c^2 = U_c^2 + U_\infty^2 v^2$, and, from equation (2.7a),

$$U_c \approx q_c = U_\infty (1 + \Sigma)^{\frac{1}{2}}. \tag{2.9}$$

Since the cavity is long and slender, the variations in the quantity ϵy_c in equation (2.8) are certainly small over most of the cavity. It is reasonable, then, to replace

the first-order small term ϵy_c with an average value $\pm\bar{\epsilon}$ on the upper and lower cavity surfaces, respectively. This averaging technique was introduced by Parkin (1957). The averaged quantity $\bar{\epsilon}$ is non-dimensional, and its value must be determined as part of the problem's solution. Equation (2.8) now becomes

$$\left.\begin{aligned} u &= \tfrac{1}{2}\Sigma+\bar{\epsilon}, \quad a \leqslant x \leqslant l \quad (y > 0),\\ u &= \tfrac{1}{2}\Sigma-\bar{\epsilon}, \quad 1 \leqslant x \leqslant l \quad (y < 0), \end{aligned}\right\} \tag{2.8a}$$

on the upper and lower cavity surfaces, respectively.

The total velocity on the solid body must be tangent to the surface of the body; hence, in terms of the perturbation velocities,

$$\frac{dy_0(x)}{dx} = \frac{v}{1+u-\epsilon y_0}.$$

After linearization the body boundary condition is

$$\frac{dy_0(x)}{dx} = \frac{v}{(1+\Sigma)^{\frac{1}{2}}} \quad (0 \leqslant x \leqslant 1). \tag{2.10}$$

This equation is also valid on the cavity surfaces and gives the surface slope at any point along the x-axis. In the cases for slender wedges and flat-plate hydrofoils,

$$\frac{dy_0(x)}{dx} = \tan\alpha \approx \alpha$$

and equation (2.10) becomes

$$v = \pm\alpha\sqrt{(1+\Sigma)} \quad (0 \leqslant x \leqslant 1), \tag{2.10a}$$

on the upper and lower wedge surfaces respectively, and

$$v = -\alpha\sqrt{(1+\Sigma)} \quad (0 \leqslant x \leqslant 1), \tag{2.10b}$$

on the solid surface of the hydrofoil. The results acquired from equations (2.8a) and (2.10) provide for smooth separation. This condition, which must be satisfied, may be thought of as equivalent to the Kutta condition in airfoil theory in that both conditions serve to single out a particular solution to the flow-boundary-value problem.

The cavity-closure condition is a characteristic of finite-cavity models. When the rotational and new irrotational flows are studied, it is seen that the subtracted portion ψ_P of the rotational flow makes no net contribution to the flow within the body-cavity area; hence, the closure condition must hold in both flows, i.e. the net strength of sources within the body-cavity area must be zero. Finally, since the basic shear flow is undisturbed at infinity, the perturbation velocities (u, v) approach zero at great distances from the body-cavity system.

The method of solution is based on the conformal mapping of the physical plane onto the exterior of the unit circle and makes use of the new harmonic flow. Following substitutions of (u, v) and ψ_P into the equations (2.1) and (2.2), these equations reduce to

$$\left.\begin{aligned} \frac{\partial v}{\partial x} &= \frac{\partial u}{\partial y},\\ \frac{\partial u}{\partial x} &= -\frac{\partial v}{\partial y}, \end{aligned}\right\} \tag{2.11}$$

respectively. In terms of the complex variable $z = x+iy$, the total complex velocity may be defined as

$$W(z) = U_\infty[1+\tfrac{1}{2}\epsilon(z-\bar{z})+w(z)]$$

with $w(z)$, the complex perturbation velocity, given by $w(z) = u-iv$. Equations (2.11) are the Cauchy–Riemann equations for $w(z)$; from these equations and the continuity of the flow, it follows that $w(z)$ is analytic outside the body-cavity system, which is represented by a slit in the z-plane, where $0 \leqslant z \leqslant l$ and z is real. Also, since $(u, v) \to 0$ at infinity, $w(z)$ must vanish at infinity. The z-plane and typical boundary conditions are shown in figure 3. Specific problems for uniform shear flow past wedges and hydrofoils, which are based on the conditions derived above, are summarized in table 1. Condition g, an additional condition, is imposed to restrict the magnitude of the singular behaviour so that the pressure distribution, which is proportional to Re (w), remains integrable.

		Wedge	Hydrofoil
D.E.		$\dfrac{\partial^2 w(z)}{\partial z\,\partial \bar{z}} = 0$	$\dfrac{\partial^2 w(z)}{\partial z\,\partial \bar{z}} = 0$
B.C.	(*a*)	$\mathrm{Re}\, w = \tfrac{1}{2}\Sigma+\bar{\epsilon},\ 1 < x \leqslant l,\ y \to 0^+$	$\mathrm{Re}\, w = \tfrac{1}{2}\Sigma+\bar{\epsilon},\ 0 \leqslant x \leqslant l,\ y \to 0^+$
	(*b*)	$\mathrm{Re}\, w = \tfrac{1}{2}\Sigma-\bar{\epsilon},\ 1 < x \leqslant l,\ y \to 0^-$	$\mathrm{Re}\, w = \tfrac{1}{2}\Sigma-\bar{\epsilon},\ 1 < x \leqslant l,\ y \to 0^-$
	(*c*)	$\mathrm{Im}\, w = -\alpha(1+\Sigma)^{\frac{1}{2}},\ 0 \leqslant x \leqslant 1,\ y \to 0^+$	None
	(*d*)	$\mathrm{Im}\, w = \alpha(1+\Sigma)^{\frac{1}{2}},\ 0 \leqslant x \leqslant 1,\ y \to 0^-$	$\mathrm{Im}\, w = \alpha(1+\Sigma)^{\frac{1}{2}},\ 0 \leqslant x \leqslant 1,\ y \to 0^-$
	(*e*)	The cavity is closed, i.e. the net source strength on the slit is zero	
	(*f*)	$w(z) \to 0$ as $z \to \infty$, i.e. $(u, v) = 0$ at infinity	
	(*g*)	$w(z)$ must not contain non-integrable singularities on the slit or have multiple values off the slit	
	(*h*)	The flow is characterized by a smooth separation from the rear of the body, i.e. $w < \infty$ at $x = 1,\ y \to 0$	

TABLE 1. Boundary-value problems for complex perturbation velocity.

In accordance with Wu (1957) and Parkin (1957), the z-plane is now mapped conformally by a succession of transforms onto the ζ-plane (figure 3). The complex velocity $w(z)$ is held invariant at corresponding points of the mappings. The transformations are listed in table 2. A complete solution $w(\zeta)$ is formed from a series of singular complex functions. These functions (familiar in airfoil theory) and their properties are listed in table 3. From figure 3, it is clear that the real parts of the singular functions must satisfy particular conditions on the real axis while the imaginary parts must satisfy other conditions on the unit circle. In addition, the limiting conditions on w as $z \to -\infty$ must be met at the corresponding points in the ζ- or Q-planes. The strength of the singularities is limited by the pressure-integrability condition previously noted. These singular functions are discussed in detail by Parkin (1957, 1959) and Wu (1956, 1957).

The solution is given in terms of the singular functions $w_i(\zeta)$ by

$$w(\zeta) = \sum_i K_i w_i(\zeta) + M + iN,$$

where the constants K_i, M, and N are real. The conditions given in table 1 serve to determine the constants and, in addition, to establish a relationship between

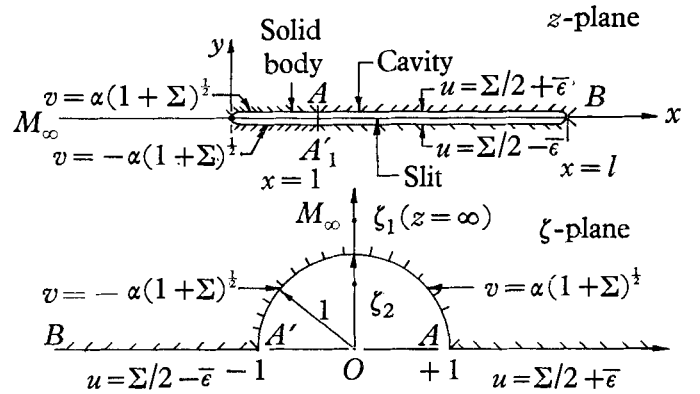

(*a*) Wedge flow

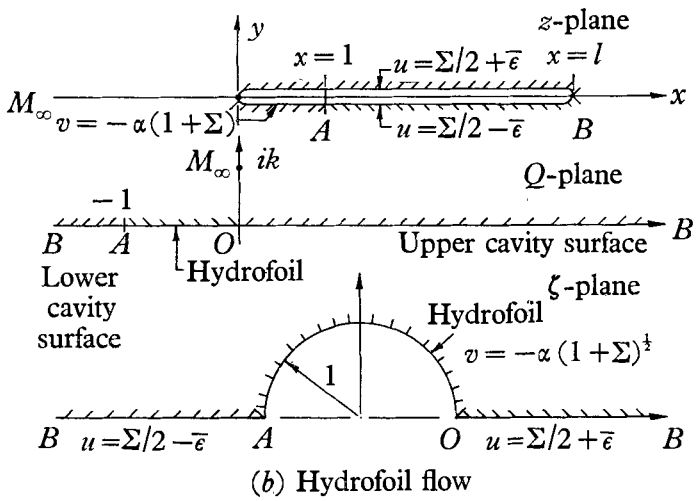

(*b*) Hydrofoil flow

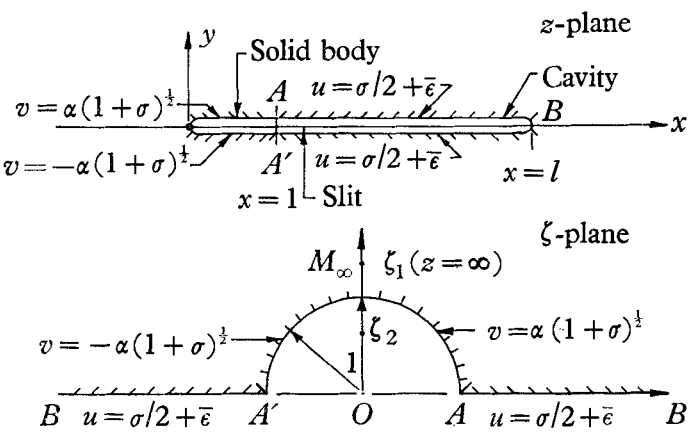

(*c*) Symmetric-wedge flow

FIGURE 3. Mapping of z-plane onto unit circle.

Σ and l, with $\bar{\epsilon}$ and α as parameters. Following the determination of w, the cavity shape and area and the pressure-force coefficients can be found by using equation (2.10) and the definitions given in the following paragraphs.

From equation (2.10), the cavity shape is given by

$$y_c(x) = (1+\Sigma)^{-\frac{1}{2}} \int_a^x v\,dx + y_0(a) \quad (a \leqslant x \leqslant l). \tag{2.12}$$

Wedge	Hydrofoil
$t = k^2 \dfrac{z}{l-z}$	(Mobius) $t = k^2 \dfrac{z}{l-z}$
$Q = t^{\frac{1}{2}} = k\left(\dfrac{z}{l-z}\right)^{\frac{1}{2}}$	(Square root) $Q = t^{\frac{1}{2}} = k\left(\dfrac{z}{l-z}\right)^{\frac{1}{2}}$
$2Q = \zeta + \dfrac{1}{\zeta}$	(Joukowsky) $2Q+1 = \dfrac{1}{2}\left(\zeta + \dfrac{1}{\zeta}\right)$
$k = (l-1)^{\frac{1}{2}}$	$k = (l-1)^{\frac{1}{2}}$

TABLE 2. Transformations.

	$w_i(\zeta)$	Purpose	Value of Re w on Im $\zeta = 0$	Value of Im w on unit circle	Remarks
1.	$\ln\dfrac{\zeta+i}{\zeta-i}$	To satisfy jump in Im (w) at nose of wedge	0	$\begin{cases} +\frac{1}{2}\pi, \text{ Re}\,\zeta > 0 \\ -\frac{1}{2}\pi, \text{ Re}\,\zeta < 0 \end{cases}$	Regular at trailing edges of wedge
2.	$i\left(\zeta - \dfrac{1}{\zeta}\right)$	Vortex pair to provide closure singularity—branching of streamlines at end of cavity	0	0	Simple poles; regular at trailing edges of wedge and hydrofoil
3.	$i\ln\zeta$	To satisfy jump in Re (w) from upper to lower cavity surfaces	$\begin{cases} 0, \zeta < 0 \\ -\pi, \zeta < 0 \end{cases}$	0	Regular at trailing edges of wedge and hydrofoil
4.	$i\dfrac{\zeta^2-1}{\zeta^2+1}$	A function symmetric about the Im (ζ) axis. To satisfy condition that $w(\zeta) \to 0$ at $\zeta_1(z = -\infty)$ in wedge flow	0	0	Equivalent to $\dfrac{i(\zeta^2-1)}{(\zeta+i)(\zeta-i)}$; a simple pole at wedge nose and regular at trailing edge
5.	$i\dfrac{1}{\zeta-1}$	Vortex at nose of hydrofoil to satisfy Im (w) = constant on foil in ζ-plane	0	$-\frac{1}{2}$	Regular at trailing edge of hydrofoil

TABLE 3. Singularities.

For wedges, $a = 1$ on both surfaces, while $y_0(1) = \pm\alpha$ on the upper and lower surfaces, respectively. For hydrofoils, $a = 0$ and $y_0(0) = 0$ on the upper cavity surface; $a = 1$ with $y_0(1) = -\alpha$ on the lower surface. Also, using (2.10), Geurst & Timman (1956) have shown that the body-cavity area S may be given by

$$S = -(1+\Sigma)^{-\frac{1}{2}} \text{Im} \oint_{\text{B+C}} wz\,dz. \tag{2.13}$$

The contour integral B+C follows a closed, counterclockwise path over the body-cavity surfaces. Recalling that $v = -\operatorname{Im} w$, one may write equation (2.12) so that

$$y_c(x) = -(1+\Sigma)^{-\frac{1}{2}} \operatorname{Im} \int_a^z w\,dz + y_0(a), \tag{2.12a}$$

where $x = z$ on the slit.

Calculation of the pressure-force coefficients is based on the pressure coefficient C_P, which is given by

$$C_P = (p-p_c)/\tfrac{1}{2}\rho U_\infty^2. \tag{2.14}$$

From equation (2.5)

$$p - p_c = \tfrac{1}{2}\rho q_c^2(1 - q_0^2/q_c^2).$$

After this relation is linearized, equation (2.14) becomes

$$C_P = -2U_c(U_0 - U_c)/U_\infty^2,$$

	Coefficient	Wedge	Hydrofoil
1.	$C_P = \dfrac{p-p_c}{\frac{1}{2}\rho U_\infty^2}$	$2(1+\Sigma)^{\frac{1}{2}}[\pm\bar{\epsilon}x + \frac{1}{2}\Sigma - u]$	$-2(1+\Sigma)^{\frac{1}{2}}[\bar{\epsilon}x + u - \frac{1}{2}\Sigma]$
2.	$C_N = \dfrac{N}{\frac{1}{2}\rho U_\infty^2\,(\text{chord})}$	—	$\displaystyle\int_0^1 C_P\,dx$
3.	$C_D = \dfrac{D}{\frac{1}{2}\rho U_\infty^2\,(\text{length})}$	$\displaystyle -\frac{1}{2\alpha}\oint_B C_P\,dy$	αC_N *
4.	$C_L = \dfrac{L}{\frac{1}{2}\rho U_\infty^2(\text{chord})}$	$\displaystyle\oint_B C_P\,dx$	C_N *
5.	$C_{MO} = \dfrac{L(\bar{x})}{\frac{1}{2}\rho U_\infty^2(\text{chord})^2}$ †	$\displaystyle\oint_B C_P\,x\,dx$	$\displaystyle\int_0^1 C_P\,x\,dx$

* Based on first-order smallness of angle of attack α.

† Taken at leading edge of body; positive in the counter-clockwise direction.

TABLE 4. Pressure-force coefficients.

where U_0 and U_c are the x-components of velocity on the solid-body and cavity surfaces, respectively. From equation (2.6a), $U_0 = U_\infty(1+u-\epsilon y_0)$ and from (2.9), $U_c = U_\infty(1+\Sigma)^{\frac{1}{2}}$; hence

$$C_P = -2(1+\Sigma)^{\frac{1}{2}}(-\tfrac{1}{2}\Sigma + u - \epsilon y_0), \tag{2.14a}$$

since $1-(1+\Sigma)^{\frac{1}{2}} \approx -\frac{1}{2}\Sigma$. In order to be consistent with the averaging approximation and to have a continuous velocity at the trailing edge, one must take $|\epsilon y| = |\bar{\epsilon}|$ on the solid body at $x = 1$. On the wedge, $y = \pm\alpha x$; hence, to the order of the approximation $\epsilon y = \pm\bar{\epsilon}x$. On the hydrofoil, $y = -\alpha x$ and $\epsilon y = -\bar{\epsilon}x$. Table 4 gives the final result for C_P and for the remaining coefficients in terms of C_P. The drag coefficient C_D is based on the base area of the wedge, i.e. 2α; the remaining coefficients use the chord of the body as a characteristic length.

From the manner in which $\bar{\epsilon}$ arises, it is reasonable to let

$$\bar{\epsilon} = \frac{\epsilon(\text{cavity area})}{2(l-1)\,(\text{chord})},$$

i.e. $\bar{\epsilon}$ equals the average value of $\epsilon\,|y|/\text{chord}$ over the cavity. On the other hand, since the vorticity creates an additional circulation, this property may be used to characterize the influence of the vorticity. (This concept was used by Parkin 1957 in his study of supercavitating flow past hydrofoils in a transverse-gravity field.) Thus, $\bar{\epsilon}$ is chosen so that the actual circulation Γ is equal to the circulation $\overline{\Gamma}$ based on the constant perturbation velocities associated with $\bar{\epsilon}$. It is convenient to balance Γ and $\overline{\Gamma}$ in terms of the harmonic velocities U_H and V_H. The resulting circulations, which are defined in the usual manner, are given to the first order in table 5. Observe that in the expression for $\bar{\epsilon}$ in table 5, the terms in the large parentheses are precisely equal to the cavity area for the wedge flow and equal to the cavity area less the triangular area between the hydrofoil and the x-axis for the hydrofoil flow. Thus, the matching of circulations at once provides a reasonably rigorous and intuitively satisfying result.

Quantity	Wedge	Hydrofoil
Γ	$\int_1^l (U_c+U_\infty \epsilon y_c)_L\,dx+\int_l^1 (U_c+U_\infty \epsilon y_c)_U\,dx$ $+\int_1^0 U_\infty(1+u)_U\,dx+\int_0^1 U_\infty(1+u)_L\,dx$	$\int_1^l (U_c+U_\infty \epsilon y_c)_L\,dx+\int_l^0 (U_c+U_\infty \epsilon y_c)_U\,dx$ $+\int_0^1 U_\infty(1+u)_L\,dx$
$\overline{\Gamma}$	$\int_1^l (U_c-U_\infty \bar{\epsilon})_L\,dx+\int_l^1 (U_c+U_\infty \bar{\epsilon})_U\,dx$ $+\int_0^1 U_\infty(1+u)_U\,dx+\int_0^1 U_\infty(1+u)_L\,dx$	$\int_1^l (U_c-U_\infty \bar{\epsilon})_L\,dx+\int_l^0 (U_c+U_\infty \bar{\epsilon})_U\,dx$ $+\int_0^1 U_\infty(1+u)_L\,dx$
$\bar{\epsilon}$	$\frac{\epsilon}{2(l-1)}\left(\int_1^l \lvert y_c\rvert_L\,dx+\int_1^l \lvert y_c\rvert_U\,dx\right)$	$\frac{\epsilon}{2(l-1)}\left(\int_1^l \lvert y_c\rvert_L\,dx+\int_0^l \lvert y_c\rvert_U\,dx\right)$

Note: The subscripts U and L refer respectively to the upper and lower surfaces of the body or cavity.

TABLE 5. Flow circulations.

3. Applications of the linearized theory

3.1. *Asymmetric flow past a wedge*

The first flow studied is a supercavitating, uniform, shear flow past a wedge. The asymmetric, undisturbed velocity profile of the flow is shown in figure 1 (solid-line profile).

The mapping of the z-plane and the appropriate boundary conditions are indicated in figure 3(*a*). By using the transformations in table 2, one can show (Acosta 1961) that

$$z = l\left[1-\frac{4(l-1)\,\zeta^2}{(\zeta^2-\zeta_1^2)\,(\zeta^2-\zeta_2^2)}\right], \tag{3.1}$$

where

$$\left.\begin{aligned}\zeta_1 &= i[l^{\frac{1}{2}}+(l-1)^{\frac{1}{2}}],\\ \zeta_2 &= i[l^{\frac{1}{2}}-(l-1)^{\frac{1}{2}}].\end{aligned}\right\} \tag{3.2}$$

The root ζ_1 is outside the unit circle and represents the point $z=\infty$.

The complex boundary-value problem for this wedge flow is given in table 1. A comparison of the boundary conditions and available singularities (table 3) shows that the solution must have the form

$$w(\zeta) = \tfrac{1}{2}\Sigma + \bar{\epsilon} - \frac{2\alpha}{\pi}(1+\Sigma)^{\frac{1}{2}} \ln\frac{\zeta+i}{\zeta-i} + i\frac{2\bar{\epsilon}}{\pi}\ln\zeta + iA\left(\zeta - \frac{1}{\zeta}\right) + iD\frac{\zeta^2-1}{\zeta^2+1}. \tag{3.3}$$

In this form w satisfies the differential equation and conditions a, b, c, d, g and h of the boundary-value problem. The remaining conditions serve to establish A and D and to determine a unique relation between l and Σ for given ϵ and α.

As Wu (1957) has pointed out, much is learned by expanding $w(z)$ in a series of the form

$$w(z) = a_0 + ib_0 + \frac{a_1+ib_1}{z} + \frac{a_2+ib_2}{z^2} + O\left(\frac{1}{z^3}\right) \tag{3.4}$$

as $z \to \infty$. As $z \to \infty$, $\zeta \to \zeta_1$; hence, by using (3.1) and (3.2), ζ can be expanded in descending powers of z. Acosta (1961) has shown that

$$\zeta = \zeta_1\left[1 + \frac{l^{\frac{1}{2}}(l-1)^{\frac{1}{2}}}{2z} + \frac{l^{\frac{1}{2}}(l-1)^{\frac{1}{2}}\{2l+1+l^{\frac{1}{2}}(l-1)^{\frac{1}{2}}\}}{8z^2} + O\left(\frac{1}{z^3}\right)\right]. \tag{3.5}$$

This result is now introduced into (3.3) and the combination is simplified. The series expansion of $w(z)$ in descending powers of z is then

$$\begin{aligned} w(z) = {} & \left\{\tfrac{1}{2}\Sigma - 2l^{\frac{1}{2}}A - \frac{\alpha(1+\Sigma)^{\frac{1}{2}}}{\pi}\ln\frac{l^{\frac{1}{2}}+1}{l^{\frac{1}{2}}-1} + \frac{i2\bar{\epsilon}}{\pi}\ln\{l^{\frac{1}{2}}+(l-1)^{\frac{1}{2}}\} - iD\frac{1+T}{1-T}\right\} \\ & + \frac{1}{z}\left\{\frac{\alpha l^{\frac{1}{2}}}{\pi}(1+\Sigma)^{\frac{1}{2}} - l^{\frac{1}{2}}(l-1)A + \frac{i\bar{\epsilon}}{\pi}l^{\frac{1}{2}}(l-1)^{\frac{1}{2}} - iD\frac{2Tl^{\frac{1}{2}}(l-1)^{\frac{1}{2}}}{(1-T)^2}\right\} \\ & + \frac{1}{z^2}\left\{\frac{\alpha}{4\pi}(1+\Sigma)^{\frac{1}{2}}l^{\frac{1}{2}}(l-1) - \frac{A}{4}(l-1)(3l+1)l^{\frac{1}{2}} + \frac{i\bar{\epsilon}}{4\pi}l^{\frac{1}{2}}(l-1)^{\frac{1}{2}}(2l+1)\right. \\ & \left. - i\frac{DT}{2(1-T)^3}[l^{\frac{1}{2}}(l-1)^{\frac{1}{2}}(1-T)\{2l+1+l^{\frac{1}{2}}(l-1)^{\frac{1}{2}}\} + l(l-1)(3T+1)]\right\} \\ & + O\left(\frac{1}{z^3}\right), \end{aligned} \tag{3.6}$$

where $\zeta_1^2 = -T = -[2l-1+2l^{\frac{1}{2}}(l-1)^{\frac{1}{2}}]$. From boundary conditions e and f one has $a_0 = a_1 = b_0 = 0$. It follows from (3.6) that, first

$$A = \alpha(1+\Sigma)^{\frac{1}{2}}/\pi(l-1) \tag{3.7a}$$

and

$$D = \frac{2\bar{\epsilon}(1-T)}{\pi(1+T)}\ln(l^{\frac{1}{2}}+(l-1)^{\frac{1}{2}}), \tag{3.7b}$$

and second, by using these results,

$$\frac{\Sigma}{(1+\Sigma)^{\frac{1}{2}}} = \frac{2\alpha}{\pi}\left[\ln\frac{l^{\frac{1}{2}}+1}{l^{\frac{1}{2}}-1} + \frac{2l^{\frac{1}{2}}}{l-1}\right]. \tag{3.8}$$

This equation is the same as that obtained by Tulin (1953) and Wu (1957) for irrotational flow past a wedge; the vorticity in the flow has no first-order effect on the cavity length.

This same conclusion can be reached by physical reasoning as follows: If a first-order length effect enters as $K\bar{e}$, then changing the sign of $\bar{e}$ reverses the first-order effect but simply inverts the flow field. Hence, a contradiction would result from the presence of a first-order length effect. This same reasoning applies to first-order changes in the drag and the cavity area, but not to changes in the other pressure-force coefficients or in the cavity shape.

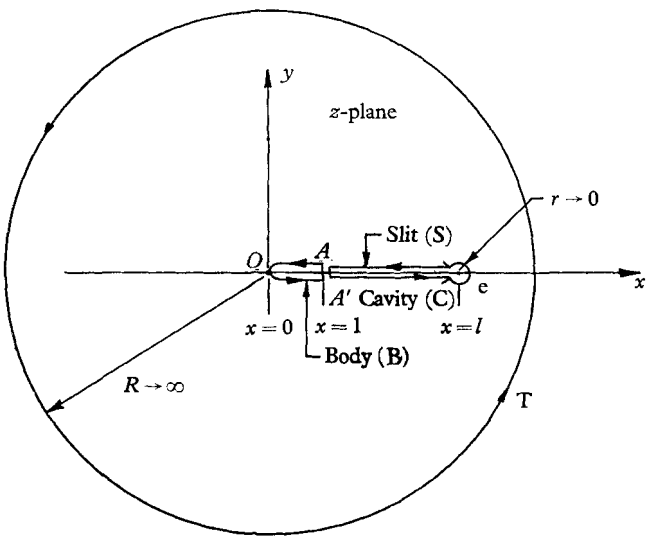

FIGURE 4. Contour paths for complex integration.

The complex perturbation velocity $w(z)$ may now be written as

$$w(z) = \frac{i\bar{e}}{2\pi} l^{\frac{1}{2}}(l-1)^{\frac{1}{2}}\left[1+\frac{4T}{T^2-1}\ln\left(l^{\frac{1}{2}}+(l-1)^{\frac{1}{2}}\right)\right]+\frac{1}{z^2}\left\{-\frac{\alpha(1+\Sigma)^{\frac{1}{2}}l^{\frac{3}{2}}}{2\pi}\right.$$
$$\left.+\frac{i\bar{e}}{4\pi} l^{\frac{1}{2}}(l-1)^{\frac{1}{2}}(2l+1)\left[1-\frac{4T\ln\left(l^{\frac{1}{2}}+(l-1)^{\frac{1}{2}}\right)}{(T^2-1)(1-T)}\left(1-T+\frac{2l^{\frac{1}{2}}(l-1)^{\frac{1}{2}}(1+T)}{2l+1}\right)\right]\right\}$$
$$+O\left(\frac{1}{z^3}\right). \tag{3.9}$$

The remaining calculations are based on equations (3.3) and (3.9).

First, the cavity area and shape are calculated. By making use of the fact that $w(z)$ is analytic off the slit, of the theory of residues, and of equation (3.4), one may write equation (2.13) as

$$S = -\frac{1}{(1+\Sigma)^{\frac{1}{2}}}\operatorname{Im}\oint_{\mathrm{T}} wz\,dz = -\frac{2\pi a_2}{(1+\Sigma)^{\frac{1}{2}}},$$

where T is a circle of large radius surrounding the slit as shown in figure 4. From (3.9),

$$a_2 = -\alpha(1+\Sigma)^{\frac{1}{2}}l^{\frac{3}{2}}/2\pi.$$

Thus
$$S = \alpha l^{\frac{3}{2}}, \tag{3.10}$$

and, since the cavity area $A_c = S-\alpha$,

$$A_c = \alpha(l^{\frac{3}{2}}-1). \tag{3.11}$$

To find the cavity shape, (2.12a) is rewritten in the form

$$y_c = \alpha - \operatorname{Im}\int_1^t \frac{w(\zeta)}{(1+\Sigma)^{\frac{1}{2}}}\frac{dz}{d\zeta}d\zeta$$

on the upper cavity surface, and

$$y_c = -\alpha - \operatorname{Im}\int_{-1}^{-t} \frac{w(\zeta)}{(1+\Sigma)^{\frac{1}{2}}}\frac{dz}{d\zeta}d\zeta$$

on the lower surface. For $|t| \geqslant 1$, one obtains from (3.1)

$$x = l\left[1 - \frac{4(l-1)t^2}{(t^2+T)(t^2+R)}\right], \tag{3.12}$$

where $T = -\zeta_1^2$ and $R = -\zeta_2^2$. The derivative $dz/d\zeta$ is found by differentiating equation (3.1). Combining the above with (3.7) and using the relation $\zeta_1^2\zeta_2^2 = 1$, one obtains the following.

On the upper cavity surface, where $t \geqslant 1$,

$$y_c = \alpha - 8l(l-1)\int_1^t \left\{\frac{\alpha}{-\pi(l-1)}\left(\zeta - \frac{1}{\zeta}\right) + \frac{2\bar{\epsilon}(1-T)}{\pi(1+T)}\left[\frac{\ln(l^{\frac{1}{2}}+(l-1)^{\frac{1}{2}})}{(1+\Sigma)^{\frac{1}{2}}}\right]\frac{\zeta^2-1}{\zeta^2+1}\right.$$
$$\left. + \frac{2\bar{\epsilon}}{\pi(1+\Sigma)^{\frac{1}{2}}}\ln\zeta - \frac{4\alpha}{\pi}\tan^{-1}\zeta\right\}\frac{\zeta(\zeta^4-1)\,d\zeta}{(\zeta^2+T)^2(\zeta^2+R)^2}, \tag{3.13a}$$

and on the lower cavity surface, where $t \leqslant 1$,

$$y_c = -\alpha + 8l(l-1)\int_1^{|t|}\left\{\frac{\alpha}{\pi(l-1)}\left(\zeta - \frac{1}{\zeta}\right) - \frac{2\bar{\epsilon}(1-T)}{\pi(1+\Sigma)^{\frac{1}{2}}(1+T)}[\ln(l^{\frac{1}{2}}+(l-1)^{\frac{1}{2}})]\frac{\zeta^2-1}{\zeta^2+1}\right.$$
$$\left. - \frac{2\bar{\epsilon}}{\pi(1+\Sigma)^{\frac{1}{2}}}\ln\zeta - \frac{4\alpha}{\pi}\tan^{-1}\zeta\right\}\frac{\zeta(\zeta^4-1)\,d\zeta}{(\zeta^2+T)^2(\zeta^2+R)^2}. \tag{3.13b}$$

Next, the pressure-force coefficients are determined. From table 4

$$C_P = 2(1+\Sigma)^{\frac{1}{2}}(\tfrac{1}{2}\Sigma - u \pm \bar{\epsilon}x) \tag{3.14}$$

on the wedge where $0 \leqslant x \leqslant 1$. Since $\zeta = e^{i\theta}$ on the wedge surfaces, the plus sign and $0 \leqslant \theta \leqslant \frac{1}{2}\pi$ apply when $y > 0$ and the minus sign and $\frac{1}{2}\pi \leqslant \theta \leqslant \pi$ apply when $y < 0$. The combination of (3.3) and (3.7) and the introduction of $\zeta = e^{i\theta}$ give, for the real part of w on the wedge,

$$u(\theta) = \tfrac{1}{2}\Sigma - \frac{2(1+\Sigma)^{\frac{1}{2}}\alpha}{\pi(l-1)}\sin\theta - \frac{2\bar{\epsilon}}{\pi}\frac{(1-T)\ln(l^{\frac{1}{2}}+(l-1)^{\frac{1}{2}})}{(1+T)}\tan\theta$$
$$+\bar{\epsilon}\left(1-\frac{2\theta}{\pi}\right) - \frac{2(1+\Sigma)^{\frac{1}{2}}\alpha}{\pi}\ln\left|\frac{1+\sin\theta}{1-\sin\theta}\right|.$$

From the transformations listed in table 2, one obtains, on the wedge,

$$x = l\cos^2\theta/(l-\sin^2\theta). \tag{3.15}$$

The above results are now introduced into (3.14) and yield

$$C_P = 2(1+\Sigma)^{\frac{1}{2}}\left\{\frac{2(1+\Sigma)^{\frac{1}{2}}\alpha}{\pi}\left[\frac{\sin\theta}{l-1} + \ln\left|\frac{1+\sin\theta}{1-\sin\theta}\right|\right]\right.$$
$$\left. + \bar{\epsilon}\left[\frac{2\theta}{\pi} - 1 + \frac{2(1-T)\ln(l^{\frac{1}{2}}+(l-1)^{\frac{1}{2}})}{\pi(1+T)}\tan\theta \pm \frac{l\cos^2\theta}{l-\sin^2\theta}\right]\right\}. \tag{3.16}$$

Equations (3.15) and (3.16) give the pressure coefficient C_P as a function of x on the wedge surfaces.

The drag coefficient is, from table 4,

$$C_D = -\frac{1}{2\alpha}\oint_{\mathrm{B}} C_P dy. \tag{3.17}$$

The contour integral B follows a closed, counterclockwise path on the wedge surfaces. When equation (3.14) is introduced into (3.17) and the relationships $dy = v(1+\Sigma)^{\frac{1}{2}}dx$ and $2uv = -\operatorname{Im} w^2$ are used, then

$$C_D = -\frac{1}{2\alpha}\left[\operatorname{Im}\oint_{\mathrm{B}} w^2 dz + 2(1+\Sigma)^{\frac{1}{2}}\oint_{\mathrm{B}}\left(\mp\bar{\epsilon}x + \frac{\Sigma}{2}\right)dy\right]. \tag{3.17a}$$

Since w is analytic off the slit, one can write

$$\oint_{\mathrm{B}} w^2 dz = \oint_{\mathrm{T}} w^2 dz - \oint_{\mathrm{C}} w^2 dz,$$

in terms of the contour paths in figure 4. The path C around the cavity on the slit consists of all the slit S (for $1 \leqslant z \leqslant l$) plus a small circle e (radius $r \to 0$) that surrounds the point $z = l$. On T, w has the form

$$w = \frac{ib_1}{z} + \frac{a_2 + ib_2}{z^2} + O\left(\frac{1}{z^3}\right),$$

so that, by the theory of residues, $\oint_{\mathrm{T}} w^2 dz = 0$. The integral over the cavity is given by

$$\operatorname{Im}\oint_{\mathrm{C}} w^2 dz = \operatorname{Im}\oint_{\mathrm{S}} w^2 dz + \operatorname{Im} J_{\mathrm{T}},$$

where J_{T} is the integral over e. It is easily shown that $\operatorname{Im}\oint_{\mathrm{S}} w^2 dz = 0$ and that $\oint_{\mathrm{B}} (\mp\bar{\epsilon}x + \frac{1}{2}\Sigma)\,dy = 0$. Thus, equation (3.17*a*) may be simplified to

$$C_D = \operatorname{Im} J_{\mathrm{T}}/2\alpha. \tag{3.17b}$$

In order to evaluate this result, w must be expanded as $z \to l$. From equation (3.1), $\zeta \to 2il^{\frac{1}{2}}(l-1)^{\frac{1}{2}}(z-l)^{\frac{1}{2}}$ as $z \to l$. Using this result, Street (1962) has shown that w has the form

$$w(z) \to -\frac{2Al^{\frac{1}{2}}(l-1)^{\frac{1}{2}}}{(z-l)^{\frac{1}{2}}} + O[\ln(z-l)^{\frac{1}{2}}] \quad \text{as} \quad z \to l.$$

Evaluation of the resulting integrals over the path e shows that

$$J_{\mathrm{T}} = \oint_{\mathrm{e}} w^2 dz = \mathrm{i}8\pi l(l-1)A^2.$$

Introducing this result and the value of A given in (3.7*a*) into equation (3.17*b*) gives the drag coefficient

$$C_D = \frac{4\alpha(1+\Sigma)l}{\pi(l-1)}. \tag{3.18}$$

As expected, this result is precisely that given by Tulin (1953) and Wu (1957) for irrotational, supercavitating flow about a slender wedge; vorticity has no first-order (order of $\bar{\epsilon}$) effect on the drag.

From table 4, the lift coefficient C_L is

$$C_L = -2(1+\Sigma)^{\frac{1}{2}} \oint_B u\,dx + 2(1+\Sigma)^{\frac{1}{2}} \oint_B (\tfrac{1}{2}\Sigma \mp \bar{\epsilon}x)\,dx.$$

The real part of $w\,dz$ is equal to $u\,dx$ on the wedge and

$$\oint_B (\tfrac{1}{2}\Sigma \mp \bar{\epsilon}x)\,dx = -\bar{\epsilon}\left[\int_0^1 x\,dx - \int_1^0 x\,dx\right] = -\bar{\epsilon}$$

so that

$$C_L = -2(1+\Sigma)^{\frac{1}{2}} \operatorname{Re} \oint_B w\,dx - 2(1+\Sigma)^{\frac{1}{2}}\bar{\epsilon}. \tag{3.19}$$

Following the same steps as in finding C_D, one obtains

$$\oint_T w\,dz = -2\pi b_1 = -2\bar{\epsilon}\{l-(l-1)\}^{\frac{1}{2}}\left[1+\frac{4T}{T^2-1}\ln\{l^{\frac{1}{2}}+(l-1)^{\frac{1}{2}}\}\right],$$

$$\operatorname{Re}\oint_S w\,dz = \oint_S u\,dx = -2\bar{\epsilon}(l-1),$$

$$\operatorname{Re}\oint_e w\,dz = 0.$$

Using these results, (3.19) can be put into the form

$$C_L = 4(1+\Sigma)^{\frac{1}{2}}\bar{\epsilon}\left\{l^{\frac{1}{2}}(l-1)^{\frac{1}{2}}\left[1+\frac{4T}{T^2-1}\ln(l^{\frac{1}{2}}+(l-1)^{\frac{1}{2}})\right]-l+\tfrac{1}{2}\right\}. \tag{3.20}$$

The moment coefficient about the nose of the wedge is defined as

$$C_{MO} = \frac{L\bar{x}}{\frac{1}{2}\rho U_\infty^2(\text{chord})^2},$$

positive in the counterclockwise direction where $\bar{x}$ is the distance to the centre of lift. Again using the results in table 4, one has

$$C_{MO} = -2(1+\Sigma)^{\frac{1}{2}}\oint_B ux\,dx + 2(1+\Sigma)^{\frac{1}{2}}\oint_B (\mp\bar{\epsilon}x+\tfrac{1}{2}\Sigma)\,x\,dx. \tag{3.21}$$

The steps that led to the determination of C_D and C_L are now repeated. One finds

$$\operatorname{Re}\oint_T wz\,dz = -2\pi b_2$$

$$= -\tfrac{1}{2}\bar{\epsilon}l^{\frac{1}{2}}(l-1)^{\frac{1}{2}}(2l+1)\left\{1+\frac{4T\ln\{l^{\frac{1}{2}}+(l-1)^{\frac{1}{2}}\}}{(T^2-1)(1-T)}\left[1-T+\frac{2l^{\frac{1}{2}}(l-1)^{\frac{1}{2}}(1+T)}{2l+1}\right]\right\},$$

$$\oint_e wz\,dz = 0 \quad \text{and} \quad \operatorname{Re}\oint_S wz\,dz = \oint_S ux\,dx = -\bar{\epsilon}(l^2-1).$$

By the introduction of these formulae, equation (3.21) can be reduced to the form

$$C_{MO} = 2(1+\Sigma)^{\frac{1}{2}}\bar{\epsilon}\left\{\frac{2l+1}{2}l^{\frac{1}{2}}(l-1)^{\frac{1}{2}}\left[1+\frac{4T\ln(l^{\frac{1}{2}}+(l-1)^{\frac{1}{2}})}{(T^2-1)(1-T)}\right.\right.$$

$$\left.\left.\times\left(1-T+\frac{2l^{\frac{1}{2}}(l-1)^{\frac{1}{2}}(1+T)}{2l+1}\right)\right]+\tfrac{1}{3}-l^2\right\}. \tag{3.22}$$

Now, from table 5,

$$\bar{\epsilon} = \frac{\epsilon}{2(l-1)}\left(\int_1^l |y_c|_L\, dx + \int_1^l |y_c|_U\, dx\right).$$

In § 2.3, it was noted that the quantity in the large parenthesis is the cavity area A_c. Thus

$$\bar{\epsilon} = \frac{\epsilon\alpha(l^2 - 1)}{2(l-1)}.$$

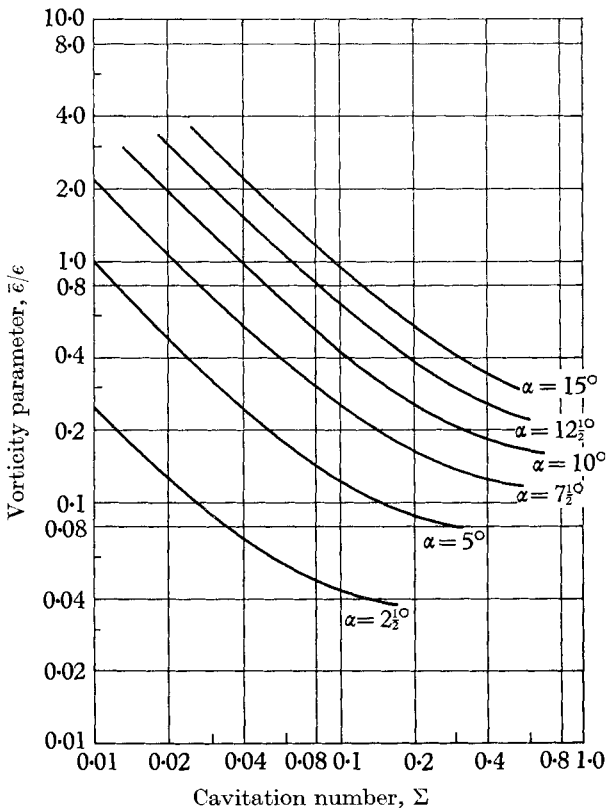

FIGURE 5. Vorticity parameter *vs* cavitation number for flow past a unit wedge.

Equation (3.23) is introduced into the previously obtained results to complete the solution to the problem.

As predicted earlier, the (l, Σ)-relation, A_c, and C_D are independent of the vorticity. On the other hand, C_L and C_{MO} depend linearly on ϵ; both coefficients are, of course, zero in the irrotational, uniform, supercavitating flow past a wedge.

Those results that are directly affected by vorticity are plotted in figures 5 to 9. The first figure shows $\bar{\epsilon}/\epsilon$ as a function of Σ. The next is a plot of typical cavity shapes; the two vorticity terms in (3.13) account for the airfoil shape of the cavity. The second, or logarithmic, term becomes large only near the end of

the cavity and tends to pull the cavity end downward. The key results of the theory are C_P, C_L and C_{MO}. Since the latter two are linear functions of ϵ, figures 7 and 8 are plotted with C_L/ϵ and C_{MO}/ϵ as functions of Σ for several values of α. The increase of both coefficients with decreasing Σ, increasing α, and increasing vorticity (or ϵ) is clearly seen. As Σ approaches zero, l, C_L and C_{MO} approach infinity. Tsien (1943) found that this behaviour also occurs in shear flow about

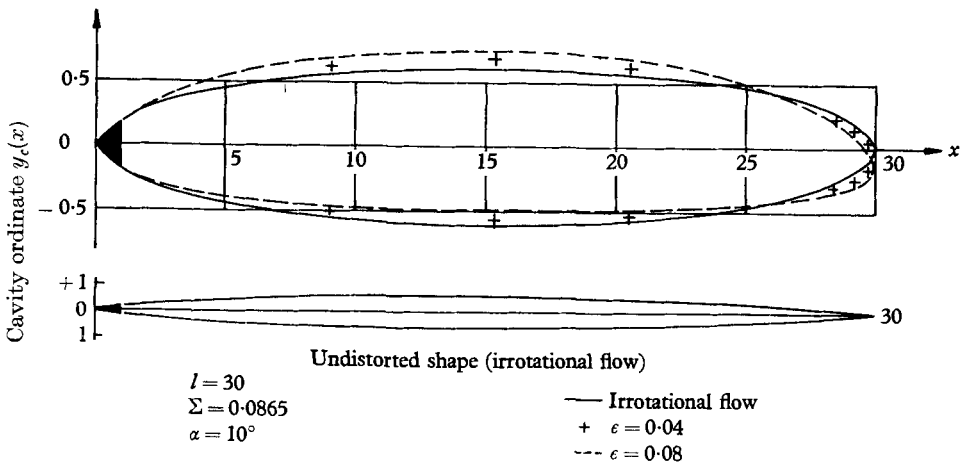

FIGURE 6. Cavity shapes at constant cavitation number in uniform shear flow past a unit wedge.

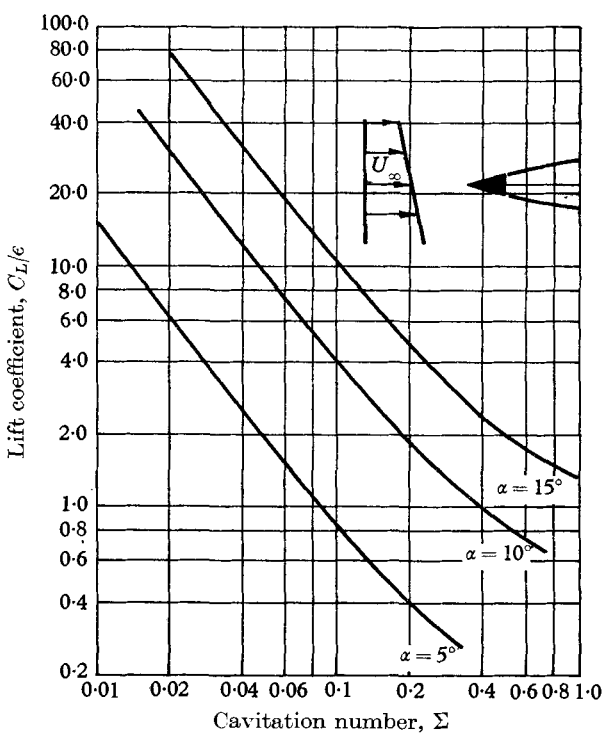

FIGURE 7. Lift coefficient for shear flow past a wedge.

an infinitely long, solid body. The pressure coefficient C_P is presented in figure 9. On the upper wedge surface near the nose, C_P exhibits a large negative value; this phenomenon is associated with the high velocities required for the fluid to turn about the sharp nose point in the equivalent non-linearized flow where the stagnation point on the wedge is below the x-axis and behind the nose. There is some experimental evidence that indicates that a small cavity actually forms in this region of low pressure.

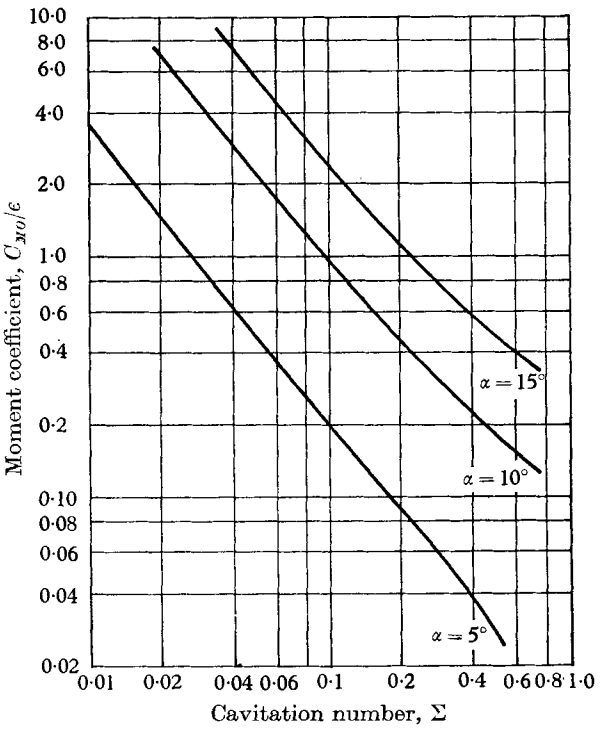

FIGURE 8. Moment coefficient for shear flow past a wedge.

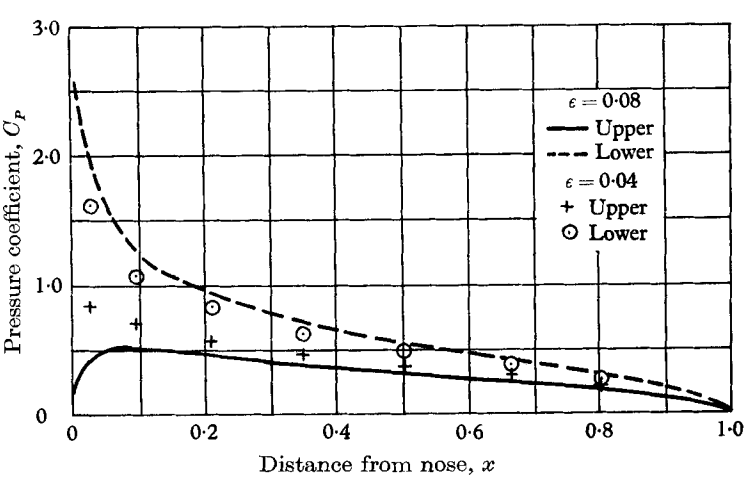

FIGURE 9. $\Sigma = 0·0865$, $l = 30$, $\alpha = 10°$ pressure coefficient for shear flow past a wedge.

3.2. *Symmetric flow past a wedge*

In symmetric flow (figure 2) Poisson's equation $\nabla^2\psi = U_\infty \epsilon$ holds for $y > 0$, but $\nabla^2\psi = -U_\infty \epsilon$ holds for $y < 0$, contrary to the asymmetric case. It becomes necessary then, to reformulate the wedge boundary-value problem outlined in table 1. However, the conformal mappings used in § 3.1 may also be used here. Furthermore, in § 2, the rotational flow was reduced to a harmonic or irrotational flow by introducing the stream function $\psi_P = U_\infty \epsilon y^2/2$. In symmetric flow, it is necessary to use $\psi_{PU} = U_\infty \epsilon y^2/2$ when $y > 0$ and $\psi_{PL} = -U_\infty \epsilon y^2/2$ when $y < 0$. The remainder of the development in § 2 is unchanged.

The boundary conditions in symmetric flow are: (*a*) the same on the upper and lower surfaces of the body-cavity combination, and (*b*) the same as those for the upper surfaces of the wedge-cavity combination in asymmetric shear flow. The new boundary conditions on the slit and the mapped planes are shown in figure 3(*c*). The mapping equation (3.1) gives z as a function of ζ as before. The boundary-value problem for symmetric flow in terms of $w = u - iv$ is the same as that given for wedge flow in table 1, except that condition (*b*) becomes

$$\operatorname{Re} w = \tfrac{1}{2}\Sigma + \bar{\epsilon} \quad (1 < x < l,\ y < 0),$$

and in symmetric flow $\Sigma = \sigma = (p_\infty - p_c)/\tfrac{1}{2}\rho U_\infty^2$.

It is seen from equation (3.3) that

$$w(\zeta) = -\frac{2\alpha}{\pi}(1+\Sigma)^{\frac{1}{2}} \ln\frac{\zeta+i}{\zeta-i} + iA\left(\zeta - \frac{1}{\zeta}\right) + \tfrac{1}{2}\Sigma + \bar{\epsilon} \tag{3.24}$$

satisfies the differential equation and conditions *a*, *b*, *c*, *d*, *g* and *h* of the revised boundary-value problem. As before, the remaining conditions serve to determine A and a relation between l and σ for fixed $\bar{\epsilon}$ and α.

By using (3.5) and (3.6) w can be expanded in the form shown in equation (3.4). The result is

$$\begin{aligned} w(z) = {} & \left[\frac{\sigma}{2} + \bar{\epsilon} - \frac{\alpha(1+\sigma)^{\frac{1}{2}}}{\pi} \ln\frac{l^{\frac{1}{2}}+1}{l^{\frac{1}{2}}-1} - 2Al^{\frac{1}{2}}\right] \\ & + \frac{1}{z}\left[\frac{\alpha(1+\sigma)^{\frac{1}{2}} l^{\frac{1}{2}}}{\pi} - A(l-1)\, l^{\frac{1}{2}}\right] \\ & + \frac{1}{z^2}\left[\frac{\alpha(1+\sigma)^{\frac{1}{2}}}{4\pi}(l+1)\, l^{\frac{1}{2}} - \tfrac{1}{4}A\,(l-1)\,(3l+1)\, l^{\frac{1}{2}}\right] + O\left(\frac{1}{z^3}\right) \end{aligned} \tag{3.25}$$

as $z \to \infty$, and since boundary conditions *e* and *f* require that $a_0 = b_0 = a_1 = 0$, it follows that

$$A = \alpha(1+\sigma)^{\frac{1}{2}}/\pi(l-1),$$

and

$$\frac{\sigma}{(1+\sigma)^{\frac{1}{2}}} = \frac{2\alpha}{\pi}\left[\ln\frac{l^{\frac{1}{2}}+1}{l^{\frac{1}{2}}-1} + \frac{2l^{\frac{1}{2}}}{l-1}\right] - \frac{2\bar{\epsilon}}{(1+\sigma)^{\frac{1}{2}}}. \tag{3.26}$$

The complex velocity $w(z)$ can now be written as

$$w(z) = -\left(\frac{\alpha(1+\sigma)^{\frac{1}{2}} l^{\frac{3}{2}}}{2\pi}\right)\frac{1}{z^2} + O\left(\frac{1}{z^3}\right). \tag{3.27}$$

The remaining calculations are based on equations (3.24) and (3.27). Since the cavity remains symmetric in shape, no lift or moments can be expected. The

quantities of interest, then, are the cavity shape, cavity area, and the pressure and drag coefficients. Only the upper wedge surface C_P and the upper cavity $y_c(x)$ need be calculated because of the flow symmetry.

The cavity area and shape are found first. From § 3.1, one has

$$\mathrm{S} = A_c + \alpha = -2\pi a_2 (1+\sigma)^{-\frac{1}{2}}.$$

Thus, as before
$$\mathrm{S} = \alpha l^{\frac{3}{2}} \tag{3.28a}$$

and
$$A_c = \alpha(l^{\frac{3}{2}} - 1). \tag{3.28b}$$

Since, as is seen in (3.26), a positive vorticity shortens the cavity length l for a fixed σ, the areas A_c and S are reduced also. The cavity shape is easily found by use of (2.12a) and several results from § 3.1. The result is

$$y_c(x) = \alpha - \frac{8\alpha l}{\pi}\int_1^t \left[\zeta - \frac{1}{\zeta} - 4(l-1)\tan^{-1}\frac{1}{\zeta}\right]\frac{\zeta(\zeta^4-1)\,d\zeta}{(\zeta^2+T)^2(\zeta^2+R)^2} \quad (t \geqslant 1). \tag{3.29}$$

As before, x is given by

$$x = l\left[1 - \frac{4(l-1)\,t^2}{(t^2+R)\,(t^2+T)}\right]. \tag{3.13c}$$

Next, the pressure and drag coefficients are determined. Following the same procedure as in § 2 yields

$$C_P = 2(1+\sigma)^{\frac{1}{2}}(\bar{\epsilon}x + \tfrac{1}{2}\sigma - u) \quad (0 \leqslant x \leqslant 1). \tag{3.30}$$

From the similar calculations in § 3.1, it follows immediately that, on the upper wedge surface,

$$C_P = 2(1+\sigma)^{\frac{1}{2}}\left[\bar{\epsilon}(x-1) + \frac{2\alpha(1+\sigma)^{\frac{1}{2}}}{\pi}\left(\frac{\sin\theta}{l-1} + \ln\left|\frac{1+\sin\theta}{1-\sin\theta}\right|\right)\right] \quad (0 \leqslant \theta \leqslant \tfrac{1}{2}\pi). \tag{3.31}$$

The drag coefficient C_D is found by utilizing the relationships developed in § 3.1 and allowing for the present symmetry of the boundary conditions; the result is

$$C_D = -\frac{1}{2\alpha}\left[\mathrm{Im}\oint_{\mathrm{w}} w^2\,dz + 2(1+\sigma)^{\frac{1}{2}}\oint_{\mathrm{w}}(\bar{\epsilon}x + \tfrac{1}{2}\sigma)\,dy\right].$$

By using the same contour integrals as before (see figure 4), one finds that

$$C_D = \frac{1}{2\alpha}\,\mathrm{Im}\oint_{\mathrm{e}} w^2\,dz - (1+\sigma)^{\frac{1}{2}}\bar{\epsilon}.$$

Comparing equations (3.3) and (3.24), one sees that

$$w(z) \to \tfrac{1}{2}\sigma + \bar{\epsilon} - \frac{2A\{l(l-1)\}^{\frac{1}{2}}}{(z-l)^{\frac{1}{2}}}$$

as $z \to l$. From this result, it follows that

$$\oint_{\mathrm{e}} w^2\,dz = J_{\mathrm{T}}$$

and
$$C_D = \frac{4\alpha(1+\sigma)\,l}{\pi(l-1)} - (1+\sigma)^{\frac{1}{2}}\bar{\epsilon}. \tag{3.32}$$

Since the circulation Γ is zero about the cavity in symmetric flow, the method of matching circulations cannot be used to determine $\bar{\epsilon}$ (a process that was successful in § 3.1). However, since $\bar{\epsilon}$ is to be a representative value of $\epsilon\,|y_c|$ over the whole cavity, it is reasonable to choose

$$\bar{\epsilon} = \frac{\epsilon A_c}{2(l-1)} = \frac{\epsilon\alpha(l^{\frac{3}{2}}-1)}{2(l-1)}, \tag{3.33}$$

i.e. the mathematical average value. Again, the value of $\bar{\epsilon}$ given by (3.33) is introduced into the previously obtained results.

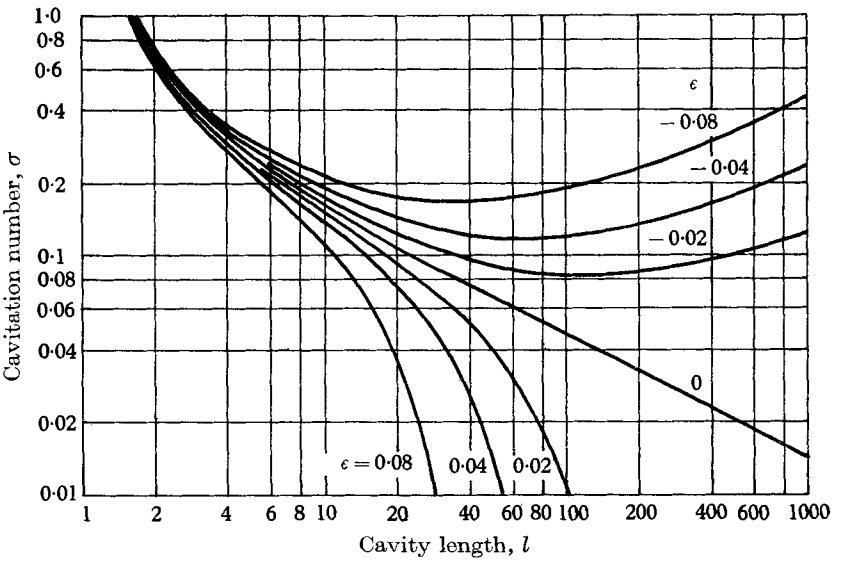

FIGURE 10. Cavitation number *vs* cavity length for symmetric shear flow past a wedge: $\alpha = 10°$.

Three important results are presented in graphical form in figures 10 to 12. First, σ is plotted as a function of l in figure 10. It is evident that positive vorticity ($\epsilon > 0$) causes a reduction in l for fixed values of σ. Although $l \to \infty$ when $\sigma \to 0$ in an irrotational flow ($\epsilon = 0$), there is a maximum l corresponding to each value of $\epsilon > 0$ in the rotational flow. When $\epsilon < 0$, the solution is no longer unique and there exists a $\sigma_{\min}$ for each ϵ. If $\sigma > \sigma_{\min}$, there are two possible cavity lengths—the conjugate lengths. Both solutions satisfy all imposed boundary conditions and produce physically reasonable C_D and cavity shapes (figures 11 and 12). Secondly, C_D is given as a function of σ for three values of ϵ when $\alpha = 10°$ in figure 11. When $\epsilon > 0$, the values of C_D for given σ and α are equal to or less than the corresponding irrotational values, and when $\epsilon < 0$, the C_D values lie on or above the comparable irrotational values. Note the reappearance of $\sigma_{\min}$ for $\epsilon < 0$ and the two possible values of C_D for each $\sigma > \sigma_{\min}$. Finally, figure 12 shows the shapes of the cavities when σ is fixed and ϵ is varied. The two longest cavities shown are the conjugate-length cavities for $\epsilon = -0{\cdot}08$.

3.3. *Asymmetric flow past a hydrofoil*

The final problem considered is a parallel, uniform, shear flow past a supercavitating, flat-plate hydrofoil as shown in figure 1. This development, which is based on the methods outlined in § 2, closely follows the development used by

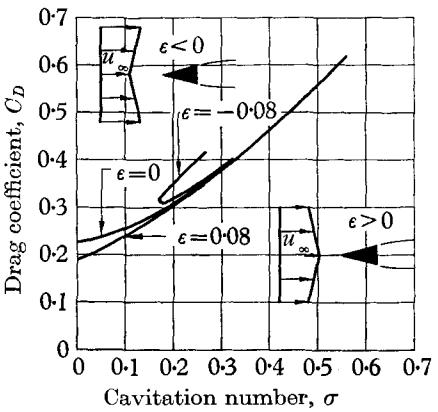

FIGURE 11. Drag coefficient *vs* cavitation number for symmetric shear flow past a wedge: $\alpha = 10°$.

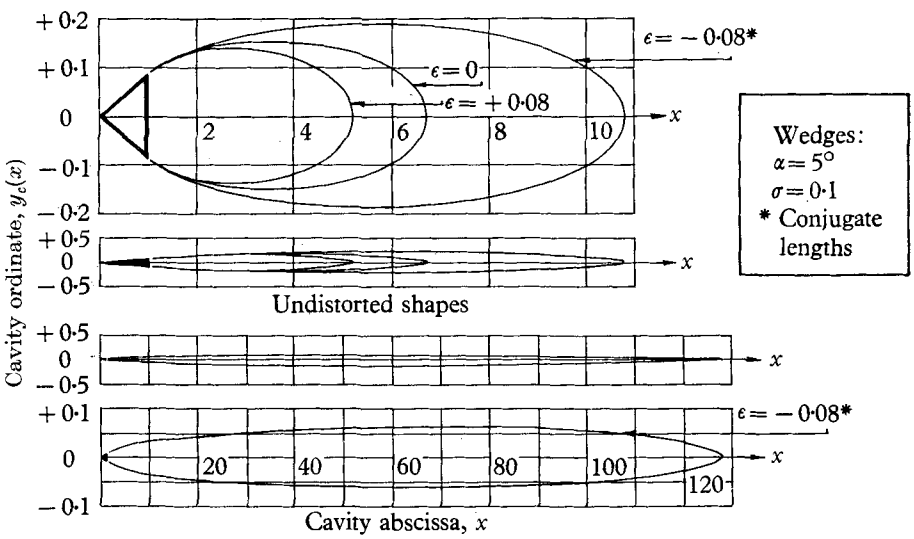

FIGURE 12. Cavity shapes for wedge in symmetric shear flow at constant cavitation number.

Parkin (1957). The basis boundary-value problems for the two flows differ only by a change in sign of the perturbation parameter. The boundary-value problem is given in table 1; the mapping transformations are listed in table 2; and the slit z-plane and transformed planes, together with corresponding boundary conditions, are shown in figure 3(*b*).

By comparing the boundary conditions and the available singularities, one can see that w should have the form

$$w(\zeta) = iA\left(\zeta - \frac{1}{\zeta}\right) + iB + iC\ln\zeta + \frac{iD}{\zeta - 1} + E. \tag{3.34}$$

The boundary conditions are now applied to this equation to determine the constants A, B, C, D and E. This application leads to the following:

$$E = \tfrac{1}{2}\Sigma + \bar{\epsilon}, \quad C = 2\bar{\epsilon}/\pi, \quad B = \alpha(1+\Sigma)^{\frac{1}{2}} + \tfrac{1}{2}D.$$

Equation (3.34) then becomes

$$w(\zeta) = iA\left(\zeta - \frac{1}{\zeta}\right) + i\alpha(1+\Sigma)^{\frac{1}{2}} + \frac{i2\bar{\epsilon}}{\pi}\ln\zeta + iD\left(\frac{1}{2} + \frac{1}{\zeta - 1}\right) + \tfrac{1}{2}\Sigma + \bar{\epsilon}. \tag{3.34a}$$

In this form, w satisfies the differential equation and all boundary conditions except e and f in table 1. These remaining conditions allow determination of A, D, and an $l - \Sigma$ relationship.

Following Parkin (1957), one completes the solution in the Q-plane (see figure 3(*b*)). From condition f, $w(z) \to 0$ and $Q \to ik$ as $z \to -\infty$. When $Q = ik$,

$$\zeta = 2ik + 1 + 2(ik - k)^{\frac{1}{2}}.$$

Letting $$r = (l^{\frac{1}{2}} + 1)^{\frac{1}{2}} + (l^{\frac{1}{2}} - 1)^{\frac{1}{2}}, \quad s = (l^{\frac{1}{2}} + 1)^{\frac{1}{2}} - (l^{\frac{1}{2}} - 1)^{\frac{1}{2}},$$

$$\lambda_1 = \ln[(1 + k^{\frac{1}{2}}s)^2 + (2k + k^{\frac{1}{2}}r)^2] \quad \text{and} \quad \lambda_2 = \tan^{-1}\frac{2k + k^{\frac{1}{2}}r}{1 + k^{\frac{1}{2}}s},$$

one obtains from (3.34*a*)

$$w(ik) = iA\left[1 + k^{\frac{1}{2}}s + i(2k + k^{\frac{1}{2}}r) - \frac{1}{1 + k^{\frac{1}{2}}s + i(2k + k^{\frac{1}{2}}r)}\right] + i\alpha(1+\Sigma)^{\frac{1}{2}}$$

$$+ iD[\tfrac{1}{2} + (k^{\frac{1}{2}}s + ik^{\frac{1}{2}}r)^{-1}] + \frac{i2\bar{\epsilon}}{\pi}\lambda_1 - \frac{2\bar{\epsilon}}{\pi}\lambda_2 + \tfrac{1}{2}\Sigma + \bar{\epsilon} = 0. \tag{3.35}$$

Equation (3.35) provides two equations for A and D. When solved simultaneously, these two equations lead to

$$A = \frac{1}{8(lk)^{\frac{1}{2}}}\left[s\left(-\frac{\bar{\epsilon}\lambda_1}{\pi} - \alpha(1+\Sigma)^{\frac{1}{2}}\right) + r\left(\bar{\epsilon} - \frac{2\bar{\epsilon}\lambda_2}{\pi} + \tfrac{1}{2}\Sigma\right)\right], \tag{3.36a}$$

and

$$D = -\left(\frac{k}{l}\right)^{\frac{1}{2}}\left[s\left(\bar{\epsilon} - \frac{2\bar{\epsilon}\lambda_2}{\pi} + \tfrac{1}{2}\Sigma\right) + r\left(\frac{\bar{\epsilon}\lambda_1}{\pi} + \alpha(1+\Sigma)^{\frac{1}{2}}\right)\right]. \tag{3.36b}$$

In the Q-plane the complex perturbation velocity is

$$w(Q) = i4AQ^{\frac{1}{2}}(Q+1)^{\frac{1}{2}} + \tfrac{1}{2}iDQ^{-\frac{1}{2}}(Q+1)^{\frac{1}{2}} + i\alpha(1+\Sigma)^{\frac{1}{2}} + \tfrac{1}{2}\Sigma$$

$$+ \bar{\epsilon} + \frac{i2\bar{\epsilon}}{\pi}\ln[1 + 2Q + 2Q^{\frac{1}{2}}(Q+1)^{\frac{1}{2}}]. \tag{3.37}$$

The remaining condition e is the closure condition, which requires that the net strength of sources within the cavity must be equal to zero or, equivalently, that $w(z)$ have no real residue within an infinitely large circle T surrounding the cavity (see figure 4), i.e.

$$\operatorname{Im}\oint_{\mathrm{T}} w\,dz = 0.$$

Because w is harmonic outside of the slit in the z-plane, it follows that

$$\operatorname{Im} \oint_{B+C} w dz = 0, \tag{3.38}$$

where B + C is the boundary of the foil-cavity system. Thus, in the Q-plane, the closure integral I_c is

$$I_c = \oint_{B+C} w(Q) \frac{dz}{dQ} dQ. \tag{3.39}$$

The foil-cavity system extends from $-\infty$ to $+\infty$ in the Q-plane. This integral is evaluated over a closed contour C_R formed by the real axis and a semicircle of radius R in the upper half plane. When $R \to \infty$, it follows immediately that

$$I_c = -2lk^2 \int_{-\infty}^{\infty} \frac{w(Q)\, Q\, dQ}{(k^2+Q^2)^2} = -2\pi i \,(\text{residues within } C_R). \tag{3.40}$$

The minus signs account for the reversal of the line integral orientation in the Q-plane. The only residue within C_R occurs at the second-order pole $Q = ik$ and is given by

$$\frac{lki}{2} \left.\frac{dw(Q)}{dQ}\right|_{Q=ik} \tag{3.41}$$

since $w(ik) = 0$. The introduction of (3.37) into (3.41) and the use of the subsequent result give

$$I_c = \tfrac{1}{8}\pi \left(\frac{l}{k}\right)^{\frac{1}{2}} \left\{ s(16k^2A + D) - 8kr\left(A + \frac{\bar{\epsilon}}{\pi}\right) - i\left[8ks\left(A + \frac{\epsilon}{\pi}\right) + r(16k^2A + D)\right]\right\}. \tag{3.42}$$

From (3.38) and (3.39), it follows that

$$8ks\left(A + \frac{\bar{\epsilon}}{\pi}\right) + r(16k^2A + D) = 0.$$

By introducing the values of the constants A and D, one derives, upon simplification, the closure condition

$$\alpha = \frac{k\Sigma}{2(1+\Sigma)^{\frac{1}{2}}} - \frac{\bar{\epsilon}}{\pi(1+\Sigma)^{\frac{1}{2}}}\left[\lambda_1 - k\pi\left(1 - \frac{2\lambda_2}{\pi}\right) - \frac{2s(kl)^{\frac{1}{2}}}{k + l^{\frac{1}{2}}}\right]. \tag{3.43}$$

As $\bar{\epsilon} \to 0$, this equation reduces to Tulin's condition for closure in the irrotational case, i.e.

$$\alpha = \tfrac{1}{2}k\Sigma(1+\Sigma)^{-\frac{1}{2}},$$

with $\Sigma = \sigma$ when $\bar{\epsilon} = 0$. When $\bar{\epsilon}$ is not zero, positive vorticity ($\epsilon > 0$) produces a lengthening of the cavity over the irrotational case for fixed α and Σ.

The cavity shape is found by integrating (2.12) directly in the Q-plane from the leading or trailing edge of the hydrofoil. The result is that

(a) on the upper cavity surface, for $q \geqslant 0$,

$$\frac{y_c}{l} = -\frac{2k^2}{(1+\Sigma)^{\frac{1}{2}}} \int_0^q \left[4AQ\,Q^{\frac{1}{2}}(Q+1)^{\frac{1}{2}} + \tfrac{1}{2}DQ^{\frac{1}{2}}(Q+1)^{\frac{1}{2}} + \alpha Q(1+\Sigma)^{\frac{1}{2}} + \frac{2\bar{\epsilon}Q}{\pi} \ln\left|1 + 2Q + 2Q^{\frac{1}{2}}(Q+1)^{\frac{1}{2}}\right|\right] \frac{dQ}{(k^2+Q^2)^2}; \tag{3.44a}$$

(*b*) on the lower cavity surface, for $|q| \geqslant 1$,

$$\frac{y_c}{l} = -\frac{\alpha}{l} + \frac{2k^2}{(1+\Sigma)^{\frac{1}{2}}} \int_1^{|q|} \left[4AQQ^{\frac{1}{2}}(Q-1)^{\frac{1}{2}} - \tfrac{1}{2}DQ^{\frac{1}{2}}(Q-1)^{\frac{1}{2}} - \alpha Q(1+\Sigma)^{\frac{1}{2}} - \frac{2\bar{\epsilon}Q}{\pi} \ln\left|1-2Q-2Q^{\frac{1}{2}}(Q-1)^{\frac{1}{2}}\right| \right] \frac{dQ}{(k^2+Q^2)^2}. \quad (3.44b)$$

These integrals, which were evaluated by Parkin (1957), are summarized in Appendix C of Street (1962). The value of x for a corresponding q is found by integrating dz/dQ and is given by

$$\frac{x}{l} = \frac{q^2}{k^2+q^2}. \quad (3.45)$$

Since the cavity and body-cavity areas are equal in this case, the cavity area A_c is, from (2.13),

$$A_c = -\frac{1}{(1+\Sigma)^{\frac{1}{2}}} \operatorname{Im} \oint_{B+C} wz\,dz.$$

The contour integral is evaluated in the Q-plane, where

$$C_c = \oint_{B+C} wz\,dz = -2k^2l^2 \oint_{C_R} w(Q) \frac{Q^3\,dQ}{(k^2+Q^2)^3}.$$

The only pole in the region is at $Q = ik$; the residue of the third-order pole there is

$$b_1 = k^2l^2 \frac{d^2}{dQ^2}\left[\frac{w(Q)\,Q^3}{(Q+ik)^3}\right]_{Q=ik}.$$

It is easily shown that $C_c = -2\pi i b_1$ and therefore that

$$C_c = -\frac{\pi(lk)^{\frac{1}{2}}}{32}\left\{4A[(6l-1)r-(12l+1)ks] + \tfrac{1}{2}D\left[r-\left(2k+\frac{3}{k}\right)s\right] + \frac{4\bar{\epsilon}}{\pi}[(4k^2+5)r+ks] + i\left(4A[kr(4k^2+5)+(2k^2+1)s] - \tfrac{1}{2}D\left[\left(2k+\frac{1}{k}\right)r-s\right] - \frac{4\bar{\epsilon}}{\pi}(kr-s)\right)\right\}. \quad (3.46)$$

Thus,

$$A_c = \frac{\pi(kl)^{\frac{1}{2}}}{8(1+\Sigma)^{\frac{1}{2}}}\left\{4A[k(4k^2+5)r+(2k^2+1)s] - \tfrac{1}{2}D\left[\left(2k+\frac{1}{k}\right)r-s\right] - \frac{4\bar{\epsilon}}{\pi}(kr-s)\right\}, \quad (3.47)$$

with A and D given by equations (3.36).

The pressure coefficient C_P, which represents the difference between the pressure p on the lower surface of the hydrofoil and the cavity pressure p_c on the upper surface, is given, from table 4, by

$$C_P = -2(1+\Sigma)^{\frac{1}{2}}(\bar{\epsilon}x - \tfrac{1}{2}\Sigma + u). \quad (3.48)$$

Since the lower side of the foil corresponds to $Q = \xi e^{i\pi}$ $(0 \leqslant \xi \leqslant 1)$, in the Q-plane, one can write

$$C_P = -2(1+\Sigma)^{\frac{1}{2}}\left[-4A\xi^{\frac{1}{2}}(1-\xi)^{\frac{1}{2}} + \tfrac{1}{2}D\xi^{-\frac{1}{2}}(1-\xi)^{\frac{1}{2}} + \bar{\epsilon}\left(1+\frac{l\xi^2}{k^2+\xi^2} - \frac{2}{\pi}\tan^{-1}\frac{2\xi^{\frac{1}{2}}(1-\xi)^{\frac{1}{2}}}{1-2\xi}\right)\right]$$
$$0 \leqslant \xi \leqslant 1 \quad \text{and} \quad \tan^{-1}[\ldots] \leqslant \pi \quad (3.49)$$

by using the given transformations and equation (3.37).

The normal force coefficient C_N is given by $C_N = \int_0^1 C_P dx$ and, from (3.48),

$$C_N = -(1+\Sigma)^{\frac{1}{2}}\left(\bar{\epsilon} - \Sigma + 2\int_0^1 u\,dx\right). \tag{3.50}$$

Writing the integral in terms of the contour integral around the cavity gives

$$\int_0^1 u\,dx = \mathrm{Re}\oint_{\mathrm{B+C}} w\,dz - \int_1^l u\,dx - \int_l^0 u\,dx.$$

The integral of w around the end of the cavity makes no contribution to the normal force; it may be shown also that the integral of wz around the end of the cavity will make no contribution to the moment. Thus, from the above and the given boundary conditions,

$$\int_0^1 u\,dx = \mathrm{Re}\oint_{\mathrm{B+C}} w(Q)\frac{dz}{dQ}dQ + \tfrac{1}{2}\Sigma + \bar{\epsilon}(2l-1).$$

The introduction of this result and (3.39) into equation (3.50) produces

$$C_N = -(1+\Sigma)^{\frac{1}{2}}[\bar{\epsilon}(4l-1) + 2\mathrm{Re}(I_c)]$$

The final form of C_N is obtained upon substitution of the known value of I_c into this result; then,

$$C_N = \frac{\pi(1+\Sigma)^{\frac{1}{2}}(l^{\frac{1}{2}}-k)}{2}\left[2\alpha k(1+\Sigma)^{\frac{1}{2}} + \Sigma + \frac{2\bar{\epsilon}}{\pi}\left(k\lambda_1 + \pi - 2\lambda_2 + \frac{2(lk)^{\frac{1}{2}}r - 4l + 1}{l^{\frac{1}{2}}-k}\right)\right]. \tag{3.51}$$

Recall that $C_L = C_N$, $C_D = \alpha C_N$, and $\alpha = D/L$.

The moment coefficient C_{MO} about the leading edge of the hydrofoil is, from table 4,

$$C_{MO} = \int_0^1 C_P x\,dx.$$

When equation (3.48) is introduced into this result, one derives

$$C_{MO} = -2(1+\Sigma)^{\frac{1}{2}}\left[\tfrac{1}{3}\bar{\epsilon} - \tfrac{1}{4}\Sigma + \int_0^1 ux\,dx\right]. \tag{3.52}$$

As before, the integral on the foil is transformed into a contour integral with the result that

$$C_{MO} = -2(1+\Sigma)^{\frac{1}{2}}\left[\bar{\epsilon}(l^2 - \tfrac{1}{6}) + \mathrm{Re}\oint_{\mathrm{B+C}} w(Q)\frac{z\,dz}{dQ}dQ\right].$$

The integral in this equation was evaluated in connexion with the determination of A_c and its value is given by the real part of equation (3.46). Hence, after minor rearrangement,

$$C_{MO} = 2(1+\Sigma)^{\frac{1}{2}}\left(\bar{\epsilon}[\tfrac{1}{8}(lk)^{\frac{1}{2}}\{(4l+1)r + ks\} - l^2 + \tfrac{1}{6}]\right.$$
$$\left. + \frac{\pi(lk)^{\frac{1}{2}}}{32}[4A\{(6l-1)r - (12l+1)ks\} + \tfrac{1}{2}D\{r - (2k+3/k)s\}]\right). \tag{3.53}$$

Finally, one determines the vorticity parameter $\bar{\epsilon}$. From table 5

$$\bar{\epsilon} = \frac{\epsilon}{2(l-1)}\left(\int_1^l |y_c|_L\, dx + \int_0^l |y_c|_U\, dx\right).$$

This result may be written as

$$\bar{\epsilon} = \epsilon(A_c - \tfrac{1}{2}\alpha)/2(l-1). \tag{3.54}$$

Recalling that (3.47) gives A_c as a function of $\bar{\epsilon}$, one can see that $\bar{\epsilon}$ may now be found directly. This calculation involves solving a quadratic relation obtained by combining (3.47) and (3.54) and using (3.44) to eliminate Σ. The result obtained is

$$\bar{\epsilon} = \frac{1}{2X_4}\left[\frac{-kX_4 + (k-\alpha)X_3}{H} + \alpha X_1 + X_2 \pm \left\{\left[\frac{-kX_4 + (k-\alpha)X_3}{H} + \alpha X_1 + X_2\right]^2 + \frac{4\alpha X_4}{H}(kX_1 + X_2)\right\}^{\frac{1}{2}}\right], \tag{3.55}$$

where

$$H = \frac{1}{\pi}\left(\lambda_1 - k\pi + 2k\lambda_2 - \frac{2(kl)^{\frac{1}{2}}s}{k + l^{\frac{1}{2}}}\right),$$

$$X_1 = \frac{\pi}{32}[2(2k^2+1)(l^{\frac{1}{2}}-1) - krs(4k^2+6)] - 1,$$

$$X_2 = \frac{\pi}{32}[2(2k^2+1)rs + k(4k^2r^2 + 5r - s^2)],$$

$$X_3 = \frac{\pi}{32}\left\{\left[\frac{r\lambda_1}{\pi} + s - \frac{2s\lambda_2}{\pi}\right][(2k^2+1)r - ks] - \left[\frac{s\lambda_1}{\pi} - r - \frac{2r\lambda_2}{\pi}\right][(4k^2+5)kr + (2k^2+1)s] - \frac{8(lk)^{\frac{1}{2}}}{\pi}(kr - s)\right\},$$

and $X_4 = 2(2l-1)/\epsilon$.

When $\epsilon > 0$ ($X_4 > 0$), the positive square root must be chosen, otherwise, $\bar{\epsilon}$ tends to a finite limit as $\epsilon \to 0^+$; this is, of course, impossible. For $\epsilon < 0$ ($X_4 < 0$), the negative square root is chosen. With $\bar{\epsilon}$ known explicitly as a function of ϵ, l (or Σ), and α, the solution is complete. The results are presented graphically in figures 13 to 21.

The cavity length l is plotted as a function of Σ for two values of α in figure 13. For a given Σ the cavity is lengthened by positive vorticity. In figure 14, the vorticity parameter is plotted *versus* Σ for various α's. A typical cavity shape is shown in figure 15. The effect of positive vorticity is seen to be an increase in cavity width and Σ for fixed l.

The force coefficients C_N and C_{MO} are pictured in figures 16 to 19. They are plotted *versus* Σ in figures 16 and 18, while they are plotted *versus* ϵ in figures 17 and 19. The rapid increase in both coefficients as Σ becomes small and l grows large is consistent with the results obtained by Tsien (1943) and those of § 3.1. The effect of the relative vorticity ϵ on C_N and C_{MO} is less pronounced except when Σ is small.

Two sets of typical pressure coefficient data are presented in figures 20 and 21. The first shows the effect of ϵ on C_P with l held constant. The second shows the effect of Σ on C_P, when α and ϵ are held constant.

Finally, from figure 13 it is seen that when $\epsilon > 0$, the solution of the problem is not unique. There is a $\Sigma_{\min}$ for each value of $\epsilon > 0$ and α. When $\Sigma > \Sigma_{\min}$,

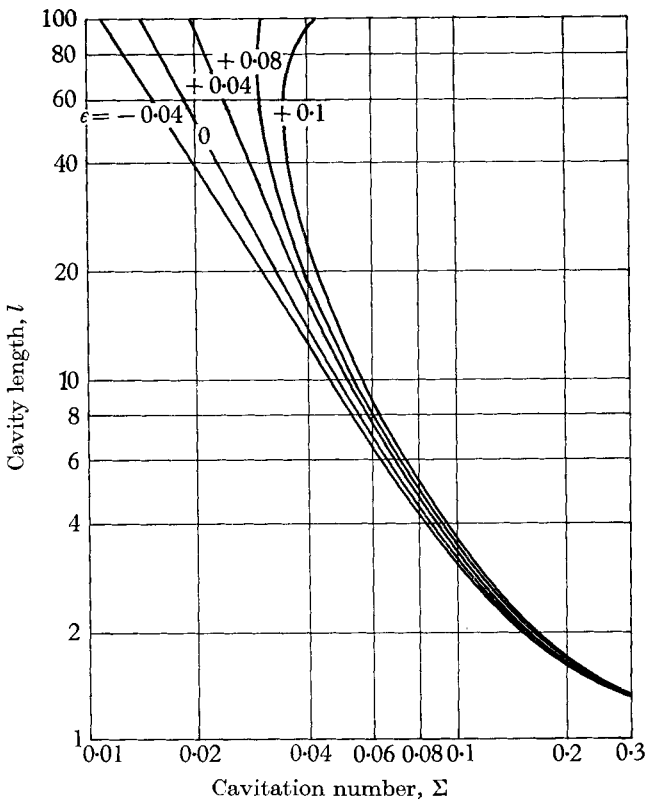

FIGURE 13. Cavity length *vs* cavitation number for shear flow past a hydrofoil: $\alpha = 4°$.

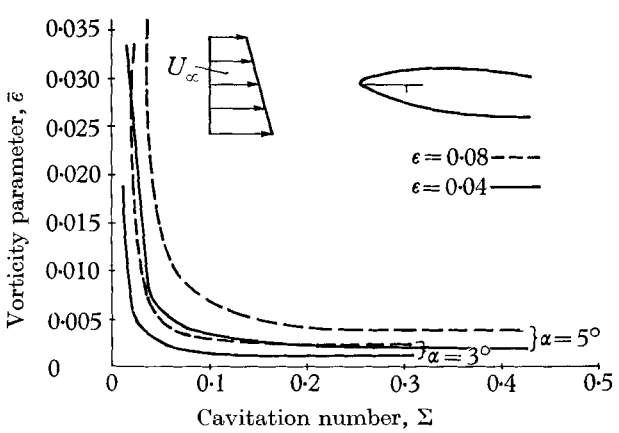

FIGURE 14. Effect of vorticity and cavitation number on vorticity parameter for shear flow past a hydrofoil.

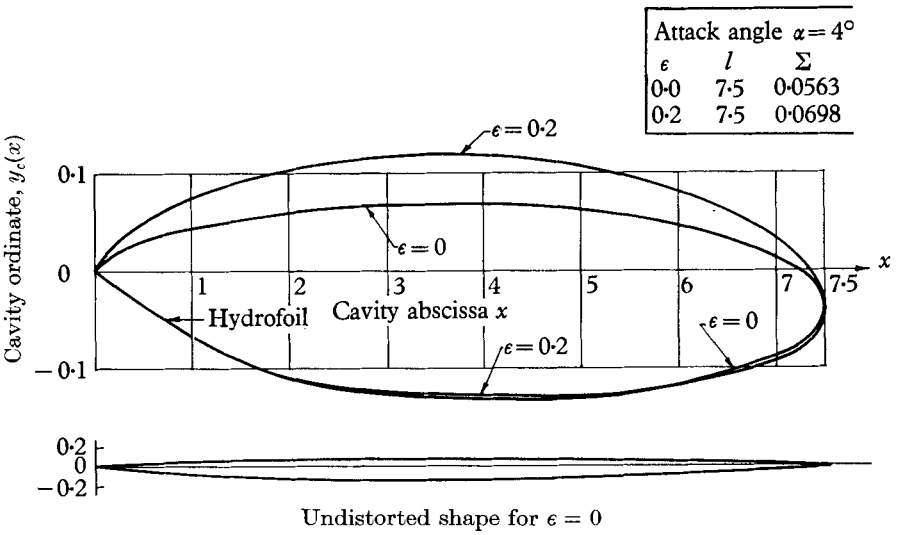

FIGURE 15. Cavity shapes at constant length in uniform shear flow.

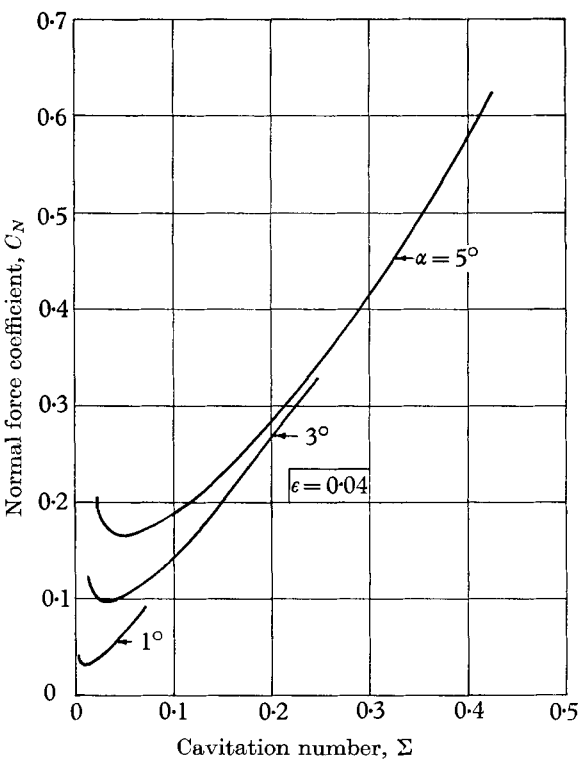

FIGURE 16. Normal force coefficient *vs* cavitation number for shear flow past a hydrofoil.

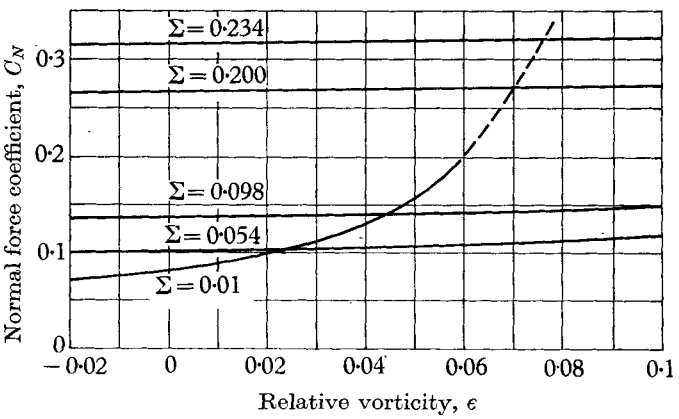

FIGURE 17. Effect of vorticity on C_N: $\alpha = 3°$ flow past a hydrofoil.

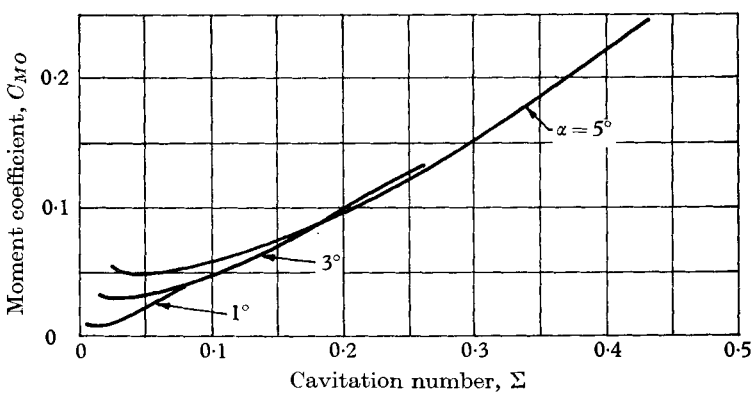

FIGURE 18. Moment coefficient *vs* cavitation number for flow past a hydrofoil at $\epsilon = 0{\cdot}04$.

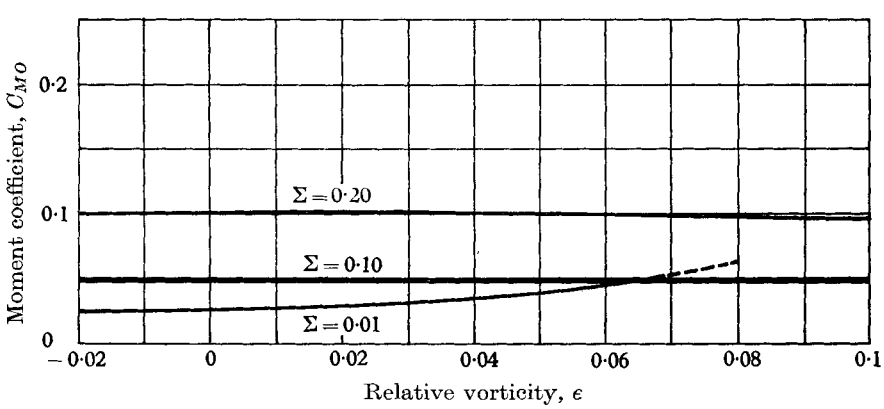

FIGURE 19. Effect of vorticity on C_{MO} at $\alpha = 3°$ for flow past a hydrofoil.

there are two possible cavity lengths—the conjugate lengths; when $\Sigma < \Sigma_{\min}$, no solution exists to the linearized problem. As in the case of symmetric flow past a wedge (§ 3.2), when two solutions do exist, they both satisfy all conditions of the problem and produce reasonable pressure force coefficients.

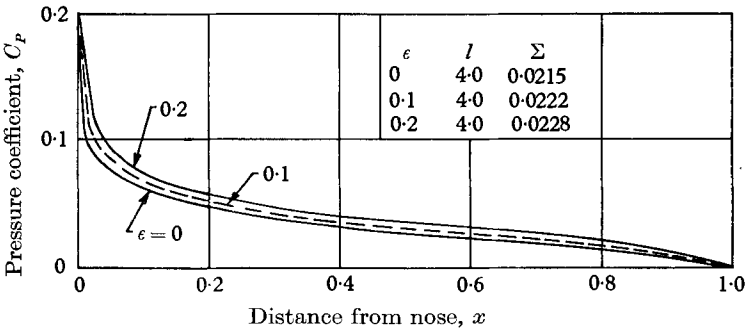

FIGURE 20. Effect of vorticity on pressure coefficient for shear flow past a hydrofoil: $\alpha = 1°$.

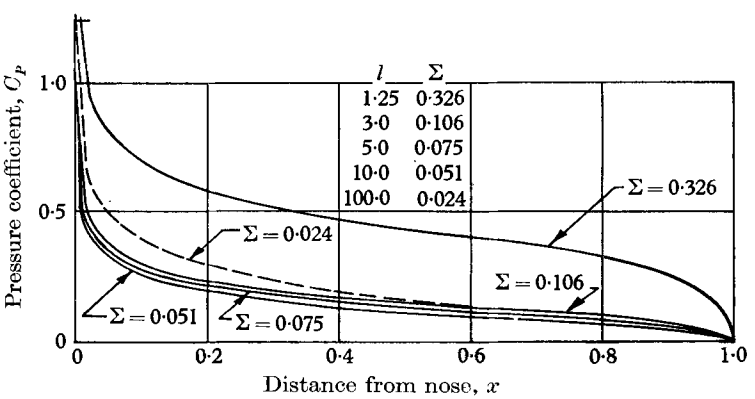

FIGURE 21. Effect of cavitation number on C_P for shear flow past a hydrofoil: $\alpha = 4°$, $\epsilon = 0·06$.

4. Concluding remarks

From the applications of the theory in § 3, it may be concluded that the effects of rotation (or vorticity) can be significant. In the cases of symmetric shear flow with negative vorticity and uniform shear flow past hydrofoils with positive vorticity, further analysis and experimentation will be required to determine if the non-unique solutions found in §§ 3.2 and 3.3 do occur.

In the uniform-shear flows about wedges and flat-plate hydrofoils, positive vorticity causes an increase in lift and moment forces; in hydrofoil flows the drag is increased also. It is important to recall the large increase in the size of vorticity effects that occur as the cavity lengthens. The work of Parkin (1957) suggests that the present linearized theory may over-estimate the vorticity effects when the cavity is extremely long. The present theory gives no indication of failure in these regions; however, as the cavity length approaches infinity, the lift and moment coefficients do become infinite.

The present application is limited in several ways. The wedge half-angles and the hydrofoil attack angles are bounded by the upper limits associated with the basic linearized theory. Chen (1962) notes that the linear theory predicts the force coefficients with an error of 8 % for a flat-plate hydrofoil at 5 degrees incidence and an error of 5 % for a symmetric wedge of 15 degrees included angle. A specific objection that may be raised is that the present theory cannot be extended directly to a higher-order accuracy, because of the averaging technique used. In addition, one must recall that $\bar{\epsilon}$ must be small compared with q_c or U_∞, and that the C_P curves must be reasonable for the theory to remain valid.

However, although the method of determining the vorticity effect is arbitrary, its value lies in the fact that it (*a*) permits solution of an otherwise difficult problem and (*b*) accounts, in general, for the over-all vorticity effects rather than the effects at one particular point in the flow.

The author expresses his appreciation to Professor Byrne Perry, Stanford University, for his help and encouragement during the course of the work. This research was carried out under the Bureau of Ships Fundamental Hydromechanics Research Program S-R009-01-01, ONR Contract Nonr 225(56). Reproduction in whole or in part is permitted for any purpose of the United States Government.

REFERENCES

Acosta, A. J. 1961 The effect of a longitudinal gravitational field on the supercavitating flow over a wedge. *J. Appl. Mech.* **28**, 188.

Chen, C. F. 1962 Second-order supercavitating hydrofoil theory. *J. Fluid Mech.* **13**, 321.

Fabula, A. G. 1962 Thin-aerofoil theory applied to hydrofoils with a single finite cavity and arbitrary free-streamline detachment. *J. Fluid Mech.* **12**, 227.

Geurst, J. A. 1961 Linearized theory of two-dimensional cavity flows. Doct. Diss., Technische Hogeschool Te Delft.

Geurst, J. A. and Timman, R. 1956 Linearized theory of two-dimensional cavitational flow around a wing section. *IXth International Congress of Appl. Mech., Brussels.*

Parkin, B. R. 1957 A note on the cavity flow past a hydrofoil in a liquid with gravity. *Calif. Inst. Tech. Engng Div. Rev.* no. 47–9.

Parkin, B. R. 1959 Linearized theory of cavity flow in two-dimension. *RAND Corp. Rep.* no. P–1745.

Street, R. L. 1962 A linearized theory for rotational, supercavitating flow. *Stanford Univ. Civil Engng Dept. Rep.* no. 16.

Tsien, H-S. 1943 Symmetrical Joukowsky airfoils in shear flow. *Quart. Appl. Math.* **1**, 130.

Tulin, M. P. 1953 Steady two-dimensional cavity flows about slender bodies. *David Taylor Model Basin Rep.* no. 834.

Wu, T. Y. 1956 A note on the linear and nonlinear theories for fully cavitated hydrofoils. *Calif. Inst. Tech. Hydro. Lab. Rep.* no. 21–22.

Wu, T. Y. 1957 A simple method for calculating the drag in the linear theory of cavity flows. *Calif. Inst. Tech. Engng Div. Rep.* no. 85–5.

Yih, C-S. 1959 Two solutions of inviscid rotational flow with corner eddies. *J. Fluid Mech.* **5**, 36.